Turkish Journal of Earth Sciences (Turkish J. Earth Sci.), Vol. 18, 2009, pp. 163–186. *Copyright ©TÜBİTAK*
doi:10.3906/yer-0802-2 First Published Online: 23 July 2008

Compositional Variations, Zoning Types and Petrogenetic Implications of Low-pressure Clinopyroxenes in the Neogene Alkaline Volcanic Rocks of Northeastern Turkey

FARUK AYDİN[1], ORHAN KARSLI[2] & M. BURHAN SADIKLAR[3]

[1] Niğde University, Department of Geological Engineering, TR–51200 Niğde, Turkey
(E-mail: faydin@nigde.edu.tr)

[2] Gümüşhane University, Department of Geological Engineering, TR–29000 Gümüşhane, Turkey

[3] Karadeniz Technical University, Department of Geological Engineering, TR–61080 Trabzon, Turkey

received 11 February 2008; revised typescript received 21 July 2008; accepted 22 July 2008

Abstract: Clinopyroxene phenocrysts and microphenocrysts in different series of the Neogene alkaline volcanic rocks from the eastern Pontides (NE Turkey) record various stages in the crystallization conditions and evolution history of the alkaline melt as well as its origin. Crystal chemical studies reveal that the clinopyroxenes in each rock series show strong textural and compositional similarities, which all reflect a common petrogenetic affinity. They have relatively high Mg-numbers (0.68–0.95), variable Al_2O_3 (1.3–9.6 wt%), low TiO_2 (<2.7 wt%) and Na_2O (<0.9 wt%) contents and low $Al^{[6]}/Al^{[4]}$ ratios (mostly <0.25), suggesting relatively low-pressure crystallization conditions of the magma in the storage region. The pressures calculated for the clinopyroxenes in each series are nearly similar and vary in the range of 2.4–4.6 ± 0.9 kbars, which approximately corresponds to a crystallization depth of 7–14 ± 3 km. The analyses of the compositional trends of the clinopyroxenes indicate the following types of zoning: (i) oscillatory and sectorial zoning related to melt crystallization (i.e. rapid cooling and crystallization), (ii) oscillatory, reverse zoning related to the different crystallization paths under a variable fluid regime, (iii) normal zoning related to the differentiation and fractional crystallization of the magma. Based on the primitive mantle- and chondrite-normalized trace and rare earth element patterns, all clinopyroxenes have high abundances of incompatible elements (i.e. La, Ce) with negative high field strength element anomalies (i.e. Zr, Ti) and low Nb/Y (0.1–0.2), Th/Y (< 0.1) and Rb/Y (< 0.03) ratios, suggesting derivation from a similar source. Obtained textural and mineral chemical data, as well as whole-rock compositions, thus suggest that the clinopyroxenes may have started to crystallize from alkaline basaltic magma derived from a homogeneous lithospheric mantle enriched by an earlier subduction event. After this process, the alkaline magma, from which early clinopyroxenes crystallized, underwent a relatively low-pressure fractional crystallization process. This was in closed magma chambers at different levels of the crust (or within a volcanic conduit system devoid of interaction processes), shown by variations in the different crystallization paths and in the fluid regime of the melt during differentiation and ascent of the magma, in a post-collisional extensional tectonic regime which affected the eastern Pontides during the Neogene.

Key Words: clinopyroxene, zoning, low-pressure, alkaline volcanics, eastern Pontides, Northeastern Turkey

Kuzeydoğu Türkiye Neojen Yaşlı Alkalin Volkanik Kayaçlarındaki Düşük Basınç Klinopiroksenlerinin Bileşimsel Değişimleri, Zonlanma Türleri ve Petrojenetik Anlamları

Özet: Doğu Pontidlerde (Kuzeydoğu Türkiye) yüzeyleyen Neojen yaşlı alkalin volkanitlerin farklı kayaç serilerindeki iri ve orta boyutlu klinopiroksen kristalleri, ana magmanın kökeni yanında, onun kristallenme şartlarının ve gelişim tarihçesinin değişik aşamalarını kaydetmiştir. Kristal kimyası çalışmaları, her bir serideki klinopiroksenlerin büyük oranda dokusal ve bileşimsel benzerlik sunduklarını ve ortak bir petrojenetik geçmişe sahip olduklarını ortaya koymuştur. İncelenen klinopiroksenler göreceli olarak yüksek Mg numarasına (0.68–0.95), değişebilir Al_2O_3 (1.3–9.6 %wt), düşük TiO_2 (<2.7 %wt) ve Na_2O (<0.9 %wt) içeriklerine ve düşük $Al^{[6]}/Al^{[4]}$ oranına (çoğunlukla <0.25) sahiptir. Dolayısıyla, bu veriler klinopiroksenlerin kristallendiği alkalen magmanın göreceli olarak düşük basınç kristallenme şartlarını destekler. Ayrıca bu klinopiroksenler için hesaplanan basınç değerleri oldukça benzerdir ve 2.4–4.6 ± 0.9 kbar arasında değişir, ki bu da yaklaşık 7–14 ± 3 km lik bir derinliğe karşılık gelir. Klinopiroksenlerin bileşimsel değişimleri aşağıdaki üç farklı zonlanma türünü ortaya koymuştur: (1) magmanın hızlı soğuması ve kristallenmesine bağlı olarak gelişen dalgalı (osilatuar) ve sektör zonlanma, (2) magmanın değişken sıvı rejimi altında farklı kristalizasyon evreleriyle ilişkili olan dalgalı-ters zonlanma, (3) magmanın kristallenme yoluyla farklılaşmasına bağlı olarak gelişen normal zonlanma. İlksel mantoya ve kondrite göre normalleştirilmiş iz ve nadir toprak element değişimlerine göre, tüm klinopiroksenler yüksek oranda uyumsuz element (La, Ce vs) içeriğine sahiptirler ve negatif yüksek alan enerjili element (Zr, Ti vs) anomalisi sunarlar. Ayrıca düşük Nb/Y (0.1–0.2), Th/Y (< 0.1) ve Rb/Y (< 0.03) oranlarına sahip olmaları, onların benzer bir manto kaynağından türemiş olduklarını gösterir. Elde edilen dokusal ve mineral kimyası verileri, tüm kayaç kompozisyonlarıyla birlikte değerlendirildiğinde, incelenen klinopiroksenlerin daha önceki bir yitimle zenginleşen homojen, litosferik bir mantodan türeyen alkalen bazaltik bir magmadan itibaren kristallenmeye başladıklarını göstermiştir. Bu süreçten sonra, erken kristallenen klinopiroksenlerin bulunduğu alkalen magma kabuğun farklı seviyelerde oluşan kapalı magma odalarında (ya da etkileşim süreçlerinden uzak bir volkanik baca içinde) düşük basınç farklılaşmasına maruz kalmıştır. Ayrıca bu klinopiroksenler, magmanın hızlı yükselimine ve farklılaşmasına bağlı olarak, değişken sıvı rejimi altında farklı kristalizasyon

evreleriyle de karşı karşıya kalmışlardır. Magmanın hızla yükselmesine muhtemelen Neojen sürecinde Doğu Pontidleri etkileyen çarpışma sonrası genişlemeye bağlı olarak oluşan tektonik rejim neden olmuştur.

Anahtar Sözcükler: klinopiroksen, zonlanma, düşük-basınç, alkalin volkanitler, doğu Pontidler, Kuzeydoğu Türkiye

Introduction

The occurrence of Ca-rich clinopyroxene phenocrysts in alkaline volcanic rocks from collision zone or post-collisional settings is generally rare and has been considered to provide important clues on the nature of crystallization and evolution of related magmas. Several studies have shown that compositional variations in the clinopyroxenes can be used as petrogenetic indicators (Dal Negro *et al.* 1982, 1986; Manoli & Molin 1988; Dobosi & Horvárth 1988; Bindi *et al.* 1999; Dobosi & Jenner 1999; Ghorbani & Middlemost 2000; Bizimis *et al.* 2000; Principalle *et al.* 2000; Nazzareni *et al.* 2001; Avanzinelli *et al.* 2004; Zhu & Ogasawara 2004). In particular, most of the clinopyroxenes in alkaline rocks show different types of zoning such as oscillatory, sector and complex (i.e. green, Fe-rich cores). Oscillatory zoning may generally indicate cyclic changes in crystallization conditions (Aurisicchio *et al.* 1988; Shimizu 1990) or different crystallization paths under a variable fluid regime (Sazonova & Nosova 1999), whereas sector zoning has a kinetic cause with differences in surface kinetic processes (adsorption-desorption) in the different growing sectors (Shimizu 1981; Watson & Liang 1995) that may indicate disequilibrium because of relatively fast crystallization. However, the changes in melt composition or physical conditions cannot be observed in the sector zoned clinopyroxenes (Nakamura 1973; Dowty 1976). Nevertheless, the origin of complex and reversed-zoned clinopyroxene phenocrysts with resorption has been ascribed to magma mixing by many researchers (e.g., Wass 1979; Duda & Shimincke 1985; Dobosi & Fodor 1992; Simonetti *et al.* 1996; Aldanmaz 2006), and this is generally called a comagmatic origin (Vollmer *et al.* 1981; Barton *et al.* 1982). In some cases, clinopyroxenes, which are not genetically related to the host lavas, are interpreted to have crystallized at high pressures from magmas, and these clinopyroxenes are called xenocrystic in origin (e.g., Shaw & Eyzaguirre 2000). In many other cases, the clinopyroxenes are in chemical equilibrium with the host lava, and their compositions provide some valuable information about magma chamber conditions and melt history prior to eruption (e.g., Liotard *et al.* 1988). Crystallization pressure of the clinopyroxenes in magmatic systems has also been investigated by several authors. Dal Negro *et al.* (1989) qualitatively discussed the influence of the crystallization pressure on the crystal-chemistry of the clinopyroxenes, and Malgarotto *et al.* (1993) also estimated the crystallization pressures of their samples using clinopyroxenes. More recently, an efficient clinopyroxene geobarometer was proposed by Nimis (1995, 1999) and Nimis & Ulmer (1998), and this provides us an opportunity to constrain the depths of magma chambers in the crust.

Neogene alkaline volcanic rocks (NAVs) containing zoned clinopyroxenes were observed in a restricted area of the East Black Sea coast in the northern zone of the eastern Pontides, NE Turkey. While there are several special studies of the whole-rock geochemistry of the alkaline rocks in this region (e.g., Çamur *et al.* 1996; Şen *et al.* 1998; Şen 2000), investigations based on mineral compositions (Hoskin *et al.* 1998a, b; Aydin 2003) and isotopic features of the rocks (Barbieri *et al.* 2000; Aydin *et al.* 2008) are few. Therefore, melt evolution and magma chamber processes during magma ascent through the Pontide crust in the Neogene remain to be discussed, and more studies of the occurrence and crystallization conditions of clinopyroxenes in Neogene alkaline volcanic rocks, northeastern Turkey, should be undertaken. This paper contributes to such studies in this region. In it, the major and trace element compositions, and zoning types of the clinopyroxenes in the potassic alkaline volcanic rocks from the northern zone of the eastern Pontides have been studied in detail in order to better understand the petrogenesis of the rocks hosting clinopyroxenes. The crystallization conditions and melt evolution history of the magma chambers in the Pontide crust are then discussed with regard to their role in the geodynamic evolution of northeastern Turkey during the Neogene.

Regional Geology

The general tectonic framework of Turkey is mainly a result of closure of the multi-branched Neotethyan Ocean during the Late Mesozoic and Cenozoic (Şengör & Kidd

1979; Şengör & Yılmaz 1981; Westaway 1994; Şengör *et al.* 2003; Rolland *et al.* 2008). However, neotectonic features of Turkey were shaped in the Neogene as a result of interactions between the northward-moving Arabian plate and the relatively stable Eurasian Plate (e.g., Şengör *et al.* 1985; Okay 1989; Yılmaz 1993; Bozkurt 2001). This neotectonic activity produced a complex set of subduction zones extending from Greece to Iran, forming several volcanic provinces of different ages and compositions (Figure 1a), namely (i) Western Anatolian Volcanic Province (WAVP), (ii) Central Anatolian Volcanic Province (CAVP), (iii) Galatian Volcanic Province (GVP), (iv) Eastern Anatolian Volcanic Province (EAVP), and (v) Northeastern Anatolian Volcanic Province (NEAVP). The NEAVP forms a considerable part of the eastern Pontides (Figure 1a), and is one of the most interesting provinces due to the presence of silica-undersaturated potassic rocks (basanite, tephrite, etc.) containing zoned clinopyroxene phenocrysts.

The eastern Pontides of Turkey, which form the eastern extension of the Sakarya terrane (Okay & Şahintürk 1997; Okay *et al.* 2008), can be basically divided into northern and southern parts, defined by different lithological and tectonic properties. The northern part is mainly dominated by Mesozoic–Cenozoic plutonic and volcanic rocks that are derived from distinct geodynamic environments, with different ages and compositions (e.g., Yılmaz & Boztuğ 1996; Şen *et al.* 1998; Karslı *et al.* 2002, 2004a, b; Aydin *et al.* 2003a, 2008; Boztuğ *et al.* 2006, 2007), while the southern zone comprises multiphase tectonic units consisting of mostly metamorphic, ophiolitic, sedimentary and subordinate magmatic rocks of pre-Cretaceous to Eocene age (e.g., Tokel 1977; Akın 1979; Eğin *et al.* 1979; Okay 1989; Yılmaz *et al.* 1997; Okay & Şahintürk 1997; Topuz & Altherr 2004; Topuz *et al.* 2004a, b, 2005). The eastern Pontides represent a well-preserved volcanic arc system, formed during the Neo-Tethyan convergence between the Afro-Arabian and Eurasian plates, which began in the early/late Cretaceous (e.g., Şengör & Kidd 1979; Şengör & Yılmaz 1981; Robinson *et al.* 1995; Yılmaz *et al.* 1997; Okay *et al.* 1997). In the late Palaeocene–early Eocene, the eastern Pontides collided with the Tauride-Anatolide platform (e.g., Keskin 2003; Şengör *et al.* 2003), and experienced long-lived collision and extension stages that resulted from crustal thickening, uplift and reheating between the early/late Eocene and the late Pliocene (e.g., Boztuğ *et al.* 2004, 2006, 2007; Karslı *et al.* 2007; Aydin *et al.* 2008). Hence, the eastern Pontides recorded a complex history of subduction-, collision- and extension-related magmatic episodes from the early/late Cretaceous to the late Neogene.

Geological and Petrological Background of the Study Area

The study area is located in the northern part of the eastern Pontides (Figure 1a), where Late Cretaceous subalkaline and Neogene alkaline volcanics (NAVs) are exposed (Figure 1b). The Late Cretaceous volcanics consist mainly of dacite with subsidiary basalt, andesite and their pyroclastic equivalents, interbedded with sedimentary rocks (Yılmaz *et al.* 2001). This series is covered by Campanian–Maastrichtian carbonates. The NAVs are the youngest volcanic unit in the study area. Previous geological (Özsayar 1987; Korkmaz 1993) and geochronological data (Hoskin & Wysoczanski 1998; Barbieri *et al.* 2000) indicate a predominantly Miocene age for the alkaline volcanism. However, recent K-Ar dates obtained from biotites in the potassic alkaline lavas around Trabzon show that the volcanic activity continued up to the late Pliocene (Aydin *et al.* 2001, 2008).

The petrographical features and whole-rock geochemistry of the NAVs, consisting of three different series [feldspar-free (Group A), feldspar and feldspathoid-bearing (Group B) and feldspathoid-free rocks (Group C)], have been well studied by Aydin (2003) and Aydin *et al.* (2008). Rocks from each series have a variable phenocryst-rich nature (14 to 63 %) with phenocryst assemblages of Cpx ± Ol ± Plag ± Foid ± Amp ± Bio + Ap + Fe-Ti oxides. However, glassy and microcrystalline groundmasses are present in some of the rocks. They have occasionally resorbed clinopyroxene (Figure 2a) and skeletal olivine (Figure 2b). The clinopyroxenes are generally euhedral-subhedral and range between 0.1 mm and 20 mm in size. They are particularly dominant in the basic members of each series, and characteristically show oscillatory (Figure 2c, d) and sector zoning (Figure 2e, f) with Mg# [$Mg/(Mg+Fe^{2+})$] of 0.68–0.95. The oscillatory zones are from a few to a several ten microns wide. The appearance of this type of zoning is controlled by the relation between diffusion rates of certain ions in the melt and the growth rate of crystals. When the latter exceeds

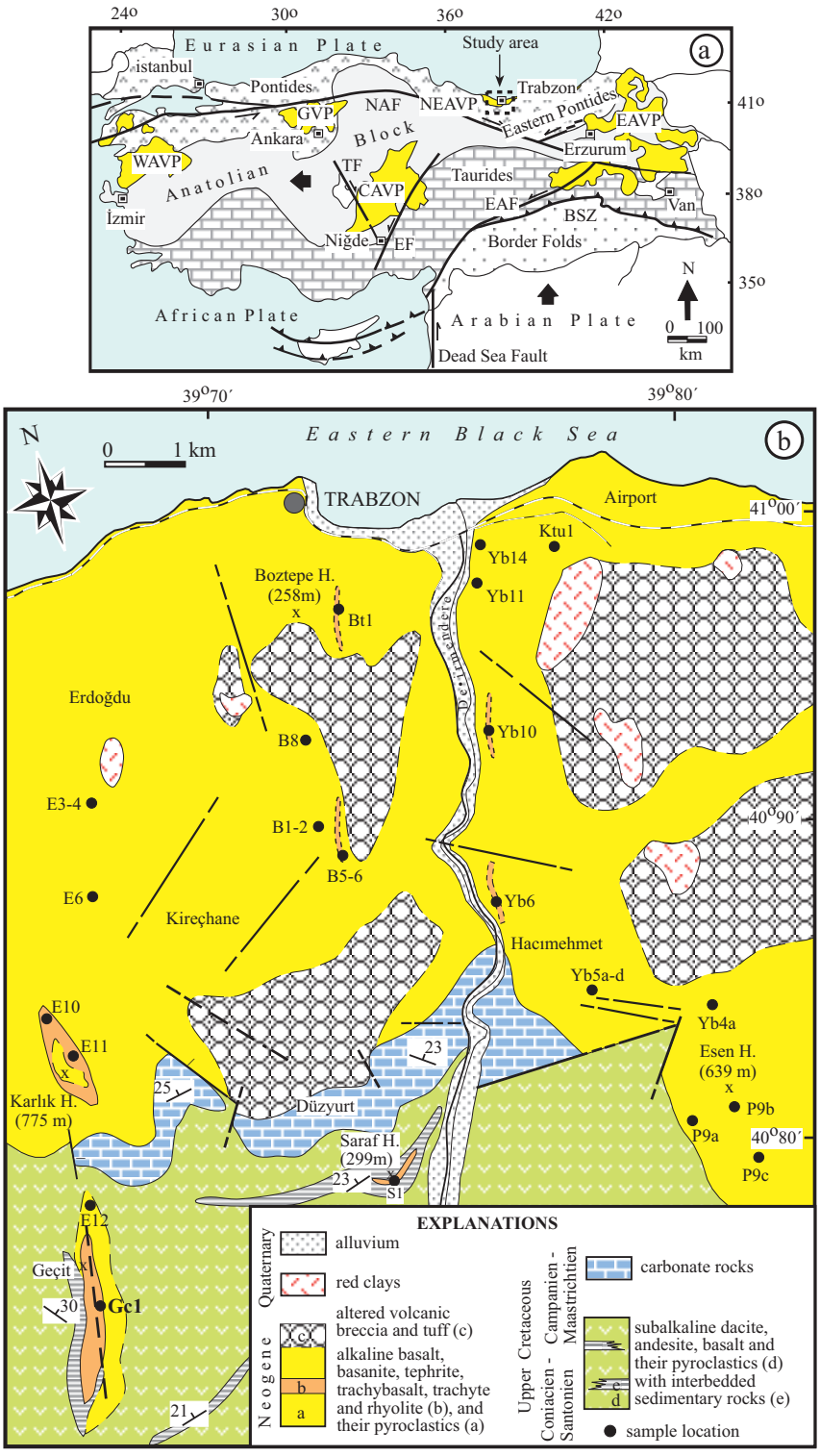

Figure 1. (a) Tectonic map of Turkey showing distribution of Neo-Quaternary volcanic provinces (modified from Bozkurt 2001); (b) simplified geological and tectonic map of the studied area with sample locations (after Aydin *et al.* 2008).

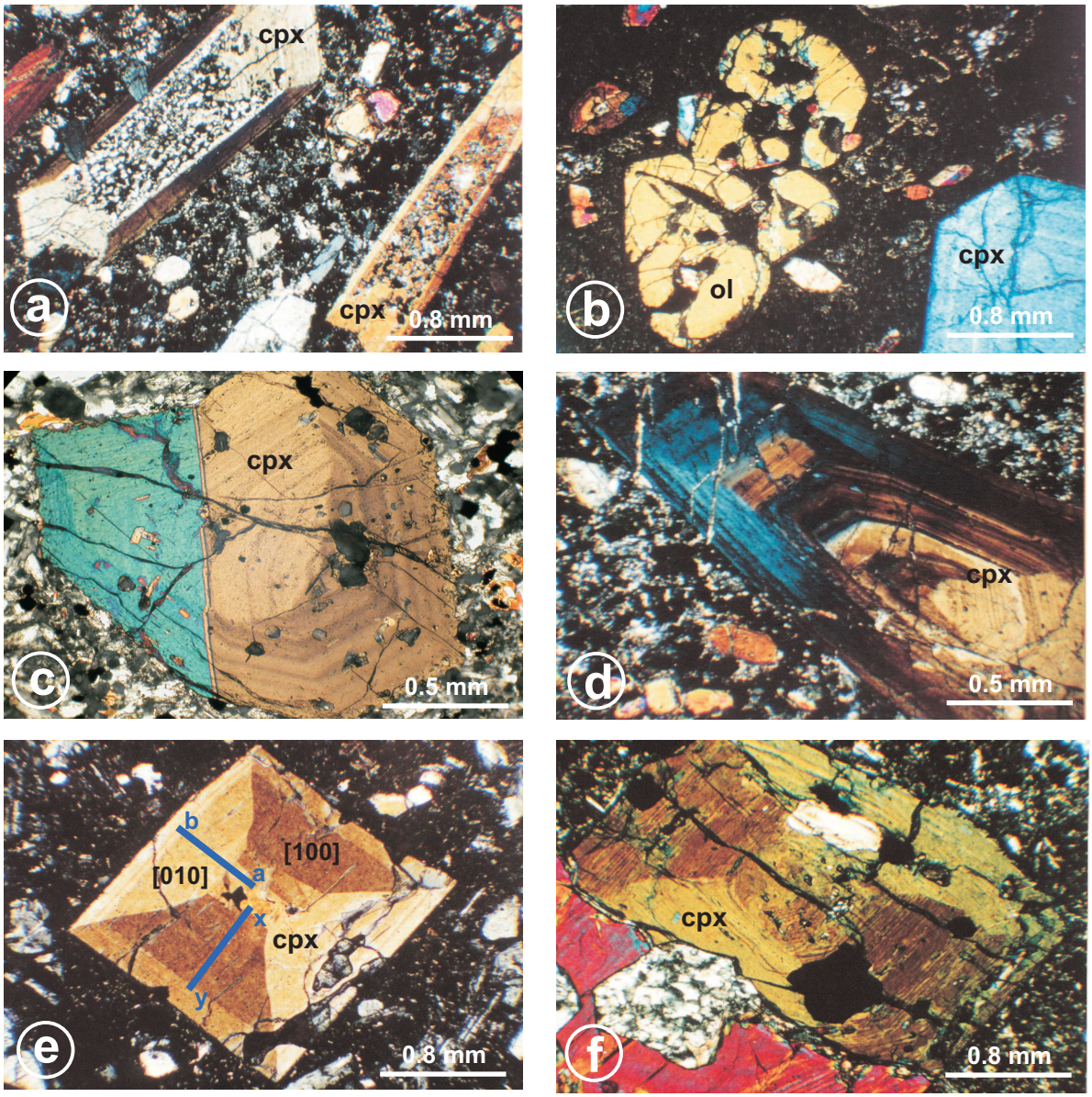

Figure 2. Petrographical microphotographs showing textural features and zoning types of clinopyroxene phenocrysts from the NAVs.

the former, the concentrations of ions in the crystal decrease and their sites in the crystal structure are occupied by another group of ions, relatively enriched in the ambient melt (Deer *et al.* 1978). However, sector zoning takes the form of four triangular segments with vertices directed toward the crystal centre (Deer *et al.* 1978). When the sector boundaries are curved, the pattern takes on an hourglass shape (Figure 2e, f). Olivine ($Fo_{91–83}$), amphibole (Mg# = 0.71–0.75) and biotite (Mg# = 0.71–0.84) have Mg-rich composition. Ca-poor ($An_{25–40}$) and Ca-rich plagioclase feldspars ($An_{51–70}$) are only present in Groups B and C. Feldspathoid minerals, generally sodalite, analcite and leucite, are found in Groups A and B. Apatite and Fe-Ti oxides are the most important accessory minerals in all series of the NAVs.

Aydin *et al.* (2008) provided detailed geochemical analyses of the NAVs. Mafic samples containing clinopyroxenes are entirely silica-undersaturated with a potassic character (Figure 3a). A Ti - (Ca+Na) diagram (Leterrier *et al.* 1982) shows that the alkalinity of the

samples changes between Group C clinopyroxenes and Group A clinopyroxenes (Figure 3b). Mg-numbers of the rocks are less than 0.5, and their Ni, Cr and Co contents range from 5 to 294 ppm, which do not approach to the values commonly assumed for primary magmas (e.g., Frey *et al.* 1978). The rocks are also characterized by high concentrations of incompatible trace elements (LILE and LREE) with negative Nb-Ta-Ti anomalies, suggesting a lithospheric mantle source, previously enriched in LILE over HFSE by the metasomatic activity of fluids released from the subducted slab (e.g., Pearce 1983; Hawkesworth *et al.* 1997; Elburg *et al.* 2002). Nd-Sr-Pb isotopic compositions for all the series of the NAVs are very similar, quite homogeneous, and have slightly depleted isotopic compositions with $_{Nd}$(13 Ma) ranging from +0.7 to +1.7 (Aydin *et al.* 2008). Young Nd model ages (T_{DM}= 0.51–0.59 Ga; Aydin *et al.* 2008) suggest that a young lithospheric mantle source, previously enriched in LIL over HFS elements, was involved in their genesis. Based on combined trace element and isotopic data, parental magmas of the eastern Pontide NAVs were apparently derived by a low proportion of partial melting from a previously enriched subcontinental lithospheric mantle source (Aydin *et al.* 2008). REE partial melting models based on metasomatised mantle (Şen 1994) also show that the alkaline rocks could be produced by 5–10% partial melting of a highly metasomatised spinel lherzolite source (Şen *et al.* 1998). Some researchers have suggested that the evolution of the alkaline volcanism was closely related to major tectonomagmatic events recognised within the tectonic framework of the eastern Pontides (e.g., Şen *et al.* 1998; Aydin *et al.* 2008).

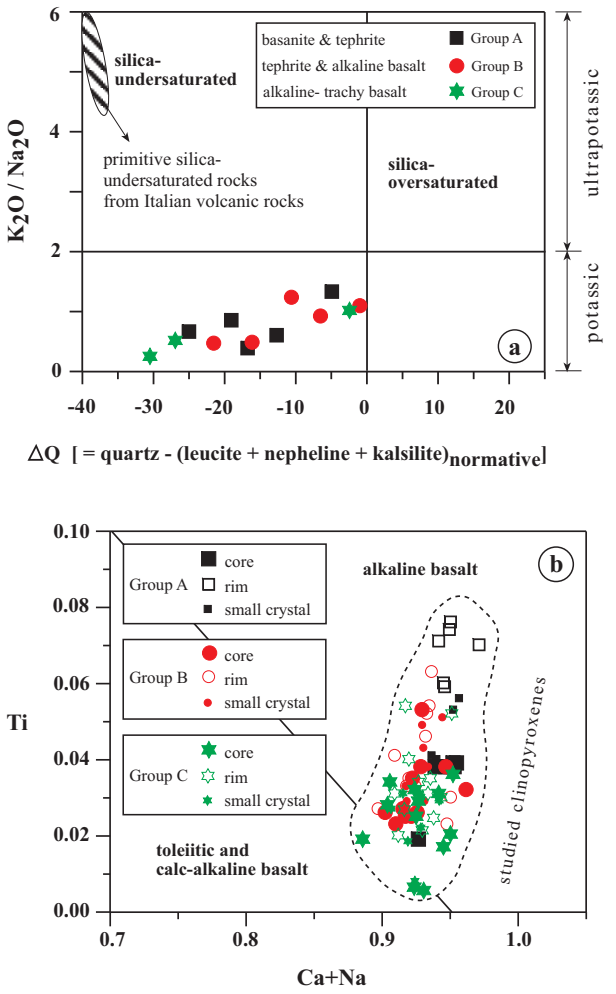

Figure 3. Classification diagrams for the rocks and studied clinopyroxenes. (a) ΔQ [= quartz – (leucite + nepheline + kalsilite)$_{normative}$] vs K_2O/Na_2O (wt %) diagram of Perini *et al.* (2004) for the host-rocks. (b) Ti vs (Ca+Na) diagram of Leterrier *et al.* (1982) for core and rim compositions of the clinopyroxenes in each series of the NAVs.

Analytical Procedures

Polished thin sections of clinopyroxenes from the NAVs were studied in detail using optical methods prior to microprobe analyses. For determination of the major element composition, a number of euhedral and subhedral clinopyroxenes were selected from eleven representative rocks; four Group A, four Group B and three Group C rock series. Chemical analyses of clinopyroxenes were performed using a CAMECA-SX-51 electron microprobe at the Mineralogical Institute of Heidelberg University, Germany. Natural and synthetic silicate standards were used. The correction procedures were performed using CAMECA's PAP software for on-line data reduction. Operating conditions were: wavelength dispersive spectrometers, 15 kV accelerating voltage, and 20 nA beam current. Beam size for these analyses was 1 μm. Fe^{3+} contents of the clinopyroxenes were calculated stoichiometrically using the equation of Droop (1987). Atomic proportions were estimated on the basis of four cations.

For trace and rare earth element analyses, four inclusion-free clinopyroxenes, without resorbtion were chosen from three rock types; i.e. from the Groups A, B and C series. Euhedral clinopyroxene phenocrysts (~0.1 cm in diameter and up to 0.5 cm long) were handpicked under the binocular and petrographic microscopes after

rock-crushing. Trace elements (Rb, Sr, Y, Zr, Nb, Cs, Ba, Hf, Ta, Pb, Th, U) and REE data were obtained by using an Elan 5000A ICP-MS at GeoForschungsZentrum Potsdam in Germany, using solution nebulisation after mixed acid digestion ($HF\text{-}HClO_4$) under pressure. Details and detection limits of the ICP-MS analysis are given in Dulski (2001). Precision for all elements is better than ± 5% and accuracy is better than ± 6%, except for Y (± 7 %) with lower relative errors than 8 %.

Results

Compositions of Clinopyroxenes

Representative major element compositions and site occupancies of the investigated clinopyroxenes are presented in Table 1. The crystals have generally high Mg numbers [$Mg/(Mg+Fe^{2+})$] of 0.68–0.95, variable Al_2O_3 (1.3–9.6 wt%), low TiO_2 (<2.7 wt%) and Na_2O (<0.9 wt%) contents and low $Al^{[6]}/Al^{[4]}$ ratios (generally <0.25). In the conventional classification diagram (Morimoto *et al.* 1988), all clinopyroxenes are diopsidic in composition (Figure 4), and most of them fall within the lower (Wo_{45}) and upper (Wo_{50}) boundaries (Figure 4), but some compositions plot above the 50% Ca line in the pyroxene quadrilateral (especially Figure 4a), as a result of high contents of non-quadrilateral components. In detail, (Figure 4a–c), clinopyroxenes from Groups A and B range in composition from Ti-rich Al-diopside (core and some small crystals) to Fe^{3+}-rich Al-diopside (i.e. Fassaite) (usually rims and a few small crystals) (Figure 4a, b), whereas clinopyroxenes from Group C fall slightly below the Wo_{50} boundary line (both phenocrysts and microcrystals of Ti-rich Al-salites, Figure 4c). Consequently, they can be classified as Ti-rich Al-diopsides (or Ti-rich Al-salites) and Fe^{3+}-rich Al-diopsides. In a Ti–$Na\text{-}Al^{[4]}$ triangular diagram (Papike *et al.* 1974), all clinopyroxene compositions completely fall in the Ca-Tschermakite molecule (CATS) field (Figure 4d) though the compositions of clinopyroxenes in Group C are more Na-rich. They contain enough Al to balance Si deficiencies in the tetrahedral sites, and their $Al^{[6]}/Al^{[4]}$ ratios are mostly ≤ 0.5 (Figure 5a). Due to Al:Ti > 5:1 (up to 10:1, Figure 5b) and good correlation of Fe^{3+} with $Al^{[4]}$ (Figure 5c), it may be inferred that Tschermak's components ($CaR^{3+}R^{3+}SiO_6$) are the most important constituents. The moderate to high Al/Ti (5.2–12.6) and low $Al^{[6]}/Al^{[4]}$ (mostly <0.25) ratios are typical of low pressure igneous clinopyroxenes (Aoki & Shiba 1973). The low Na contents indicate that the clinopyroxenes in the NAVs are poor in acmite.

In the clinopyroxenes of each series, the Al^{3+} content is high and present mostly in the T site and to a lesser extent in the M1 site (Table 1), as in clinopyroxenes from the potassic alkaline volcanic province in Italy (Bindi *et al.* 1999; Avanzinelli *et al.* 2004). The M1 site is dominated by Mg (0.515–0.842 a.f.u.) with minor amounts of Fe^{2+} (0.029–0.246 a.f.u.) and R^{3+} ($Al^{VI}+Fe^{3+}+Cr^{3+}+Ti^{4+}$ = 0.060–0.342 a.f.u.). The M2 site is almost fully occupied by Ca (0.884–0.964 a.f.u.), while Na (<0.065 a.f.u.), Mn (<0.021 a.f.u.) and Mg_{M2} (<0.039 a.f.u.) are characteristically low (Table 1). In all clinopyroxenes, Al_t is sufficient to completely fill the deficiency of Si^{4+} in the tetrahedral sites. Differences observed in the Fe^{3+} content can be explained by different oxidation states or diverse oxygen fugacities of the magmas (Canil & Fedortchouck 2000; Aydin 2008).

The Fe/Mg exchange partition coefficient (K_d) between clinopyroxene and basaltic liquid is well constrained in several experimental studies (e.g., Grove *et al.* 1982; Sisson & Grove 1993; Toplis & Carrol 1995). In Figure 6, some Mg-numbers (Mg#) of clinopyroxenes (both phenocryst cores and rims and groundmass crystals) plotted against the Mg# of whole-rock compositions reveal whether or not the clinopyroxenes are in equilibrium with their host rock. This figure also shows the equilibrium field for Fe/Mg exchange between clinopyroxene and basaltic melt (0.23 ± 0.05; Toplis & Carrol 1995). Clinopyroxenes in Group A are entirely in equilibrium, with liquids compositionally similar to their host rocks as the equilibrium partitioning of Mg and Fe between clinopyroxene and liquid remains within the range of 0.18–0.28 (Figure 6). In Group B samples, when comparing the samples in equilibrium with those in disequilibrium, the samples in disequilibrium are the clinopyroxenes with higher Mg#. While core compositions in the Group C samples are in disequilibrium, the rim and groundmass compositions are in equilibrium.

Zoning Types in Clinopyroxenes

Representative chemical data for zoning types in the clinopyroxenes are given in Table 2. Analyzing along a rim to rim profile of clinopyroxene phenocrysts (Figure 7a–c), we recognized the following types of zoning: (i) zoning

Table 1. Representative chemical compositions and site occupancies of clinopyroxenes from each series of the NAVs.

	Feldspar-free Rock Series (Group A)								Feldspar- and Feldspathoid-bearing Rocks Series (Group B)							
	Basanite			Ol-tephrite		Tephrite			Tephrite			Phonotephrite				
	P9a-1-r	5-c	9-sc	Yb5d-2-r	5-c	Ktu1-1-r	12-c	10-sc	Yb6-1-r	13-c	25-sc	Yb10-1-r	2-c	10-sc	E10-2-r	5-c
SiO_2	43.21	47.51	48.64	43.24	47.47	43.73	50.79	48.51	47.27	46.09	46.35	46.84	47.66	46.53	46.66	48.68
TiO_2	2.71	1.33	1.38	2.37	1.24	1.72	0.67	0.92	1.15	1.23	1.87	1.64	1.17	1.33	1.32	0.88
Al_2O_3	9.09	5.64	4.98	9.07	6.13	8.26	4.13	5.12	6.73	7.51	6.99	6.81	5.13	6.77	5.90	6.09
Cr_2O_3	0.03	0.02	0.06	0.01	0.00	0.03	0.16	0.00	0.01	0.03	0.06	0.01	0.02	0.01	0.02	0.14
Fe_2O_3	8.58	5.68	5.44	0.00	5.11	7.23	3.29	5.41	6.19	7.04	5.29	5.08	5.34	5.65	5.68	3.63
FeO	1.35	1.58	1.75	8.18	1.90	3.77	1.40	1.56	1.86	1.12	3.07	2.69	4.15	3.90	3.75	3.41
MnO	0.12	0.08	0.15	0.09	0.09	0.19	0.11	0.13	0.17	0.24	0.26	0.24	0.38	0.28	0.17	0.08
MgO	11.20	13.42	13.89	11.34	13.06	10.24	15.64	13.96	13.11	12.58	12.40	12.52	11.78	11.50	11.95	13.35
CaO	23.59	23.74	23.95	23.45	23.84	23.54	23.75	23.63	22.11	22.40	22.63	22.95	22.96	22.86	22.99	23.02
Na_2O	0.52	0.43	0.45	0.40	0.44	0.32	0.32	0.43	0.80	0.80	0.58	0.60	0.66	0.61	0.49	0.46
K_2O	0.02	0.00	0.00	0.00	0.01	0.01	0.01	0.00	0.04	0.00	0.00	0.01	0.00	0.02	0.01	0.03
Sum	100.42	99.43	100.69	98.15	99.29	99.04	100.27	99.67	99.44	99.04	99.50	99.39	99.25	99.46	98.94	99.77
Site T																
Si	1.621	1.774	1.793	1.670	1.774	1.672	1.857	1.802	1.763	1.729	1.738	1.754	1.801	1.754	1.768	1.807
Al	0.379	0.226	0.207	0.330	0.226	0.328	0.143	0.198	0.237	0.271	0.262	0.246	0.199	0.246	0.232	0.193
Site M1																
Mg	0.623	0.649	0.758	0.647	0.726	0.589	0.657	0.762	0.706	0.660	0.690	0.668	0.676	0.653	0.655	0.731
Fe^{2+}	0.035	0.150	0.042	0.232	0.051	0.108	0.195	0.035	0.029	0.044	0.059	0.089	0.109	0.094	0.113	0.066
Mn	0.000	0.000	0.000	0.000	0.000	0.000	0.000	0.000	0.000	0.000	0.000	0.000	0.000	0.000	0.000	0.000
Fe^{3+}	0.242	0.147	0.151	0.000	0.144	0.208	0.090	0.151	0.174	0.199	0.149	0.143	0.152	0.160	0.162	0.101
Al	0.023	0.015	0.009	0.080	0.044	0.044	0.035	0.026	0.059	0.061	0.047	0.054	0.029	0.055	0.031	0.073
Cr	0.001	0.001	0.002	0.000	0.000	0.001	0.004	0.000	0.000	0.001	0.002	0.000	0.001	0.000	0.001	0.004
Ti	0.076	0.038	0.038	0.070	0.035	0.050	0.019	0.026	0.032	0.035	0.053	0.046	0.033	0.038	0.038	0.025
Site M2																
Ca	0.948	0.950	0.946	0.950	0.955	0.964	0.930	0.940	0.884	0.900	0.910	0.921	0.930	0.923	0.933	0.915
Na	0.038	0.031	0.032	0.030	0.032	0.023	0.023	0.031	0.058	0.058	0.042	0.044	0.049	0.044	0.036	0.033
Mn	0.004	0.002	0.005	0.000	0.003	0.003	0.003	0.004	0.005	0.008	0.008	0.008	0.012	0.009	0.005	0.003
Fe^{2+}	0.007	0.017	0.012	0.025	0.008	0.010	0.044	0.014	0.030	0.034	0.037	0.026	0.009	0.024	0.026	0.041
Mg	0.003	0.000	0.005	0.000	0.002	0.000	0.000	0.011	0.023	0.000	0.003	0.001	0.000	0.000	0.000	0.008
Wo	50.91	49.61	49.30	49.56	50.56	51.22	48.46	49.03	47.76	48.78	49.03	49.62	49.26	49.54	49.26	49.06
En	33.62	33.89	39.76	33.75	38.54	31.30	34.24	40.32	39.38	35.77	37.34	36.05	35.81	35.05	34.58	39.62
Fs	15.47	16.50	10.94	16.69	10.91	17.48	17.30	10.64	12.86	15.45	13.63	14.33	14.94	15.41	16.16	11.31
R^{3+}	0.342	0.201	0.200	0.150	0.223	0.303	0.148	0.203	0.265	0.296	0.251	0.243	0.215	0.253	0.232	0.203
Mg#	0.937	0.795	0.933	0.716	0.925	0.833	0.733	0.940	0.923	0.894	0.878	0.853	0.851	0.847	0.825	0.872

Structural formulae calculated on the basis of six oxygens, Mg# = (Mg/Mg+Fe^{2+}), R^{3+}= (Al^{VI}+Fe^{3+}+Cr^{3+}+Ti^{4+}) and partitioning of Fe^{2+} and Mg at M1 and M2, respectively were done according to *Dal Negro et al.* (1982).

Table 1. Continued.

	Feldspathoid-free Series (Group C)								
	Alkaline basalt		Trachybasalt			Trachyte			
	E6-6-1-r	6-c	13-sc	P9b-1-r	3-c	10-sc	E12-1-r	5-c	21-sc
SiO_2	45.27	50.19	53.13	47.77	48.41	49.35	47.48	49.84	48.19
TiO_2	1.42	0.62	0.30	1.44	1.19	1.22	1.16	0.76	1.00
Al_2O_3	7.91	3.93	1.35	5.95	5.70	4.84	6.77	4.68	4.12
Cr_2O_3	0.04	0.00	0.00	0.00	0.00	0.00	0.06	0.03	0.00
Fe_2O_3	6.29	4.41	1.10	5.09	4.36	4.38	5.06	4.78	7.47
FeO	3.58	3.86	4.40	2.56	3.51	3.22	3.09	1.51	2.04
MnO	0.22	0.16	0.24	0.21	0.15	0.17	0.11	0.11	0.23
MgO	11.00	12.92	15.24	13.25	13.49	14.01	12.64	14.16	12.65
CaO	23.09	23.02	23.42	22.63	22.44	22.46	23.31	22.80	23.04
Na_2O	0.52	0.86	0.41	0.65	0.54	0.64	0.48	0.78	0.89
K_2O	0.00	0.02	0.03	0.01	0.00	0.00	0.00	0.20	0.02
Sum	99.34	99.99	99.62	99.56	99.79	100.29	100.16	99.65	99.65
Site T									
Si	1.712	1.866	1.962	1.781	1.800	1.823	1.765	1.842	1.808
Al	0.288	0.134	0.038	0.219	0.200	0.177	0.235	0.158	0.192
Site M1									
Mg	0.625	0.719	0.842	0.726	0.738	0.759	0.550	0.593	0.515
Fe^{2+}	0.090	0.103	0.098	0.048	0.057	0.051	0.211	0.206	0.246
Mn	0.000	0.000	0.000	0.000	0.000	0.000	0.000	0.000	0.000
Fe^{3+}	0.179	0.123	0.031	0.143	0.122	0.122	0.142	0.133	0.211
Al	0.065	0.038	0.021	0.043	0.050	0.034	0.062	0.046	0.000
Cr	0.001	0.000	0.000	0.000	0.000	0.000	0.002	0.001	0.000
Ti	0.040	0.017	0.008	0.040	0.033	0.034	0.033	0.021	0.028
Site M2									
Ca	0.936	0.917	0.927	0.904	0.894	0.889	0.928	0.903	0.926
Na	0.038	0.062	0.029	0.047	0.039	0.046	0.035	0.056	0.065
Mn	0.007	0.005	0.008	0.006	0.005	0.005	0.004	0.003	0.007
Fe^{2+}	0.019	0.016	0.036	0.033	0.052	0.047	0.000	0.000	0.000
Mg	0.000	0.000	0.000	0.010	0.010	0.013	0.033	0.038	0.002
Wo	50.43	48.70	47.73	48.34	47.6	47.14	49.68	48.13	48.56
En	33.67	36.18	43.36	39.36	35.83	40.93	31.21	33.64	27.11
Fs	15.89	13.12	8.91	12.30	12.57	11.93	19.11	18.23	24.33
R^{3+}	0.285	0.178	0.060	0.226	0.205	0.190	0.239	0.201	0.239
Mg#	0.851	0.858	0.863	0.900	0.871	0.886	0.723	0.742	0.677

related to crystallization of melt (oscillatory and sectorial zoning), (ii) zoning related to different crystallization paths under a variable fluid regime (oscillatory, reverse zoning), (iii) zoning related to fractionation of crystallizing magma (normal zoning, i.e. enrichment of Fe, Al and Ti in at rims). The zoning types are presented in detail below.

(I) Oscillatory and sectorial zoning were commonly observed in clinopyroxenes from Groups A and B. The oscillations were clearly distinguished by their different colours under the optical microscope (Figure 7a, b), and as back-scattered electron images they are light and dark zones that will be referred to as light and dark zones, respectively. The light zones are enriched in Fe^{2+}, Ca, Al and Ti and depleted in Mg and Si (not shown) compared with the dark zones (Figure 7a, b). In contrast, clinopyroxenes from Groups A and B (Figure 2e, f) often display sectorial zoning (sometimes called hourglass zoning). The opposing sectors are chemically identical, whereas adjacent ones ([100] and [010]) have different compositions and different colours under the optical microscope;

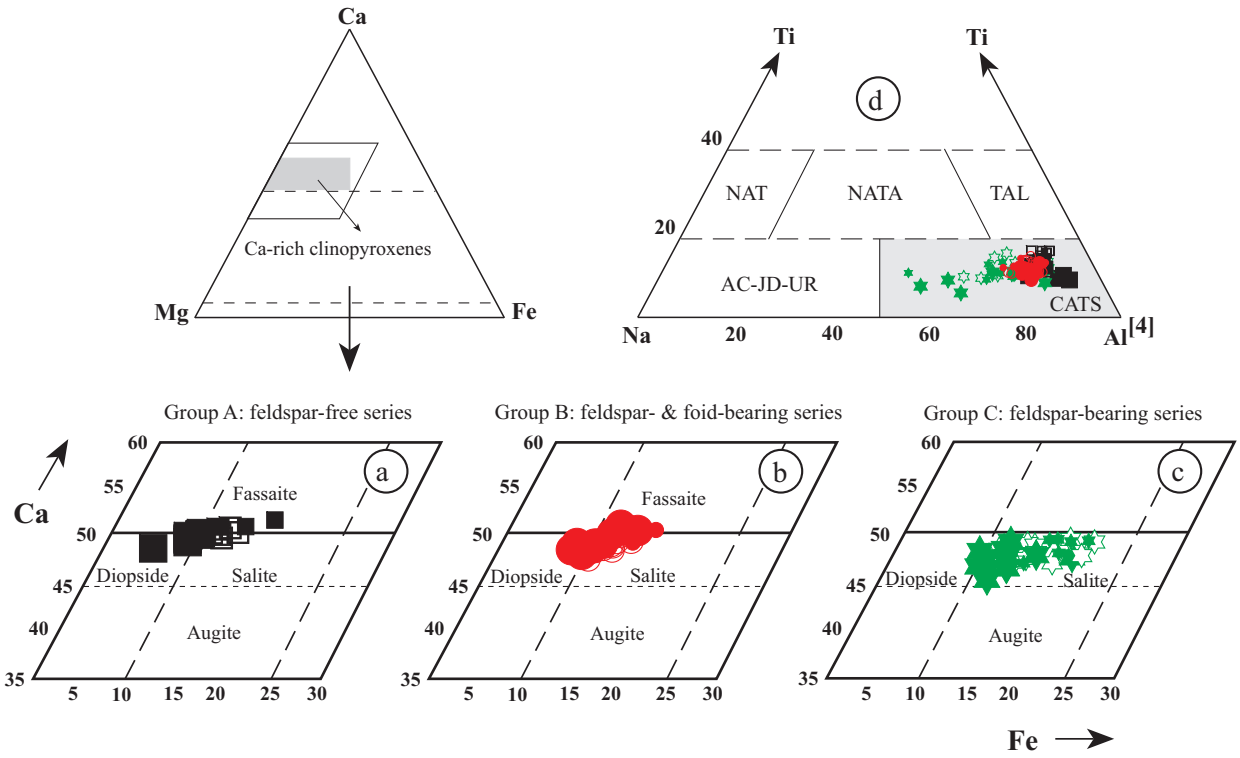

Figure 4. (a–c) Clinopyroxene compositions plotted on a Ca-Mg-Fe triangular diagram. (a) Group A rocks; clinopyroxenes from the feldspar-free rocks; (b) Group B rocks; clinopyroxenes from the feldspar-and feldspathoid-bearing rocks; (c) Group C rocks; clinopyroxenes from feldspathoid-free rocks; (d) Ti-Na-Al[4] plot (after Papike *et al.* 1974) of all the clinopyroxenes where NAT– $NaTi_{0.5}R_{0.5}^{2+}Si_2O_6$; NATAL– $NaTiSiAlO_6$; TAL– $CaTiAl_2O_6$; CATS– $CaAlAlSiO_6$ and $CaFeAlSiO_6$; Ac– $NaFeSi_2O_6$; JD– $NaAlSi_2O_6$; UR– $NaCrSi_2O_6$. The symbols and explanations in each series show the core and rim compositions of clinopyroxene phenocrysts, and small crystals in the groundmass.

each sector may also display oscillatory zoning (Figure 2f). Specifically, the [100] sector is enriched in Si and Mg (Figure 8a, b), and depleted in Ti, Al (Figure 8c, d), and Fe^{2+} and Na (not shown) relative to the [010] sector, a characteristic similar to sector-zoned titanaugite phenocrysts from alkaline rocks worldwide (e.g., Downes 1974; Shimizu 1981; Shearer & Larsen 1994).

(II) Oscillatory, reverse zoning was occasionally observed in clinopyroxenes from Groups A and B (Figure 7a). In particular, Group A clinopyroxenes consist of three distinct parts compared with those from Group B: core, intermediate zone and rim. The core has a nearly homogenous composition, characterized by lower Mg content and by higher Fe, Al and Ti concentrations. In the intermediate zone, the trends become reversed (i.e. reversed zoning): Mg gradually increases whereas Fe, Al and Ti relatively decrease rimward. An increase in the Mg concentration with the decrease of Fe and a simultaneous increase in Si with the decrease of Al reflect an inversion of the crystallization direction. The third compositional part of the profiles is a very thin clinopyroxene rim that has a nearly homogenous composition in terms of all the elements. Consequently, Group A clinopyroxenes show evidence of three crystallization stages: (i) the crystallization of the core, (ii) the crystallization of the intermediate zone, and (iii) the crystallization of the rim. The three stages, in our opinion, reflect the change from constant to different crystallization paths and probably reflect the following three stages in the crystallization of the melt: (1) relatively low-pressure (P ≈ 3–4 kbars) crystallization under a constant fluid regime, (2) different crystallization paths under a variable fluid regime, (3) stable crystallization in hypabyssal settings (~2 kbars) devoid of sudden changes in the intensive parameters. In contrast, Group B clinopyroxenes show no evidence of three crystallization stages

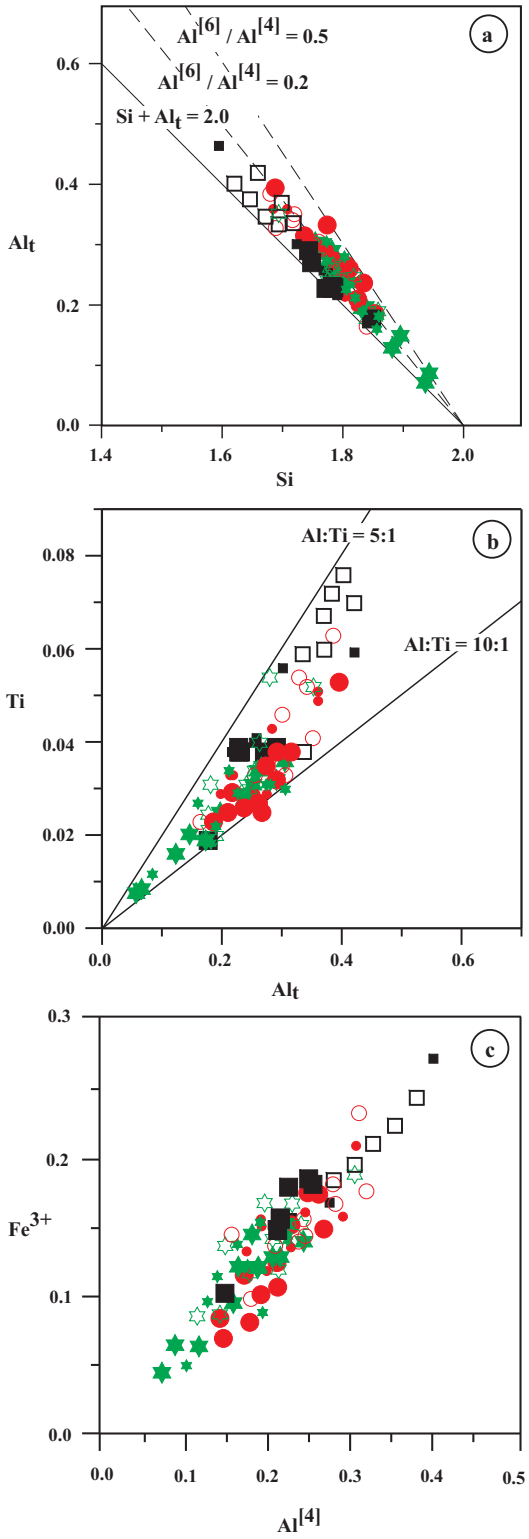

Figure 5. (a) Al_t versus Si, (b) Ti versus Al_t and (c) Fe^{3+} versus $Al^{[4]}$ diagrams for the studied clinopyroxenes. Cations are per formula unit (a.f.u.). Symbols are as in Figure 3b.

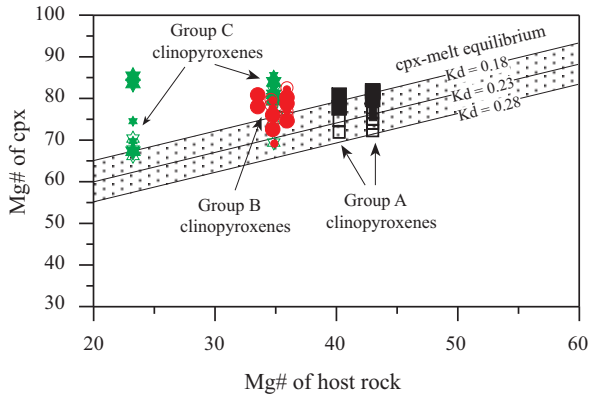

Figure 6. Equilibrium Mg# [100*Mg/(Mg+Fe^{2+})] of liquid calculated from clinopyroxene compositions versus Mg# of host-rock samples (FeO= 0.85*Fe_2O_3) for the alkaline volcanic rocks of northeastern Turkey. The shaded area represents equilibrium between clinopyroxene and host-rock composition. K_d values ($^{Fe/Mg}Kd_{min/liq}$) are from Toplis & Carrol (1995).

because they have a nearly homogenous composition across the crystal (Figure 7b).

(III) Normal zoning is usually observed in Group C clinopyroxenes. As can be seen in compositional profiles across the crystal (Figure 7c), this phenocryst shows generally normal zoning with enrichment of Fe^{2+}, Al and Ti from core to rim compared to the other clinopyroxenes, which is the direct result of magmatic fractionation. However, it consists of three distinct regions: core, mantle and rim. The core has a nearly homogeneous composition. It is characterized by higher Mg and Ca concentrations and lower contents of Fe, Al and Ti (Figure 7c), most commonly developed in relatively deep-seated quiet environments (<15 km) devoid of sudden changes in the intensive parameters of the magmatic system. The mantle shows strong oscillatory zonation, clearly distinguishable from the core (Figure 7c). The oscillatory zoning shows an overall increasing trend of Fe, Al, and Ti and decreasing concentration trend of Mg and Ca throughout the mantle. Finally, the rim is nearly homogeneous, with relative enrichment of Mg and Ca. Consequently, these characteristics record a normal process of melt fractionation and variations in the crystallization conditions of the clinopyroxenes. The mantle and rim of the clinopyroxenes from the Group C crystallized in near-surface environments (~5–6 km depth).

Table 2. Representative chemical compositions for oscillatory- and sector-zoning in clinopyroxene phenocrysts.

	Oscillatory-zoned Cpx Phenocryst				Sector-zoned Cpx Phenocryst							
					[100] sector				*[010] sector*			
	rim			core	rim			core	rim			core
	Ktu1-1	Ktu1-4	Ktu1-7	Ktu1-10	Ktu1-12	Yb6-1	Yb6-3	Yb6-5	Yb6-8	Yb6-2	Yb6-4	Yb6-6
SiO_2	43.73	50.47	48.22	49.32	50.79	47.27	47.80	46.96	48.14	46.24	45.68	43.78
TiO_2	1.72	0.73	1.11	0.74	0.67	1.15	1.23	1.28	1.25	1.45	1.78	2.16
Al_2O_3	8.26	4.05	6.06	5.14	4.13	6.73	5.77	7.22	6.23	8.00	8.17	9.62
Cr_2O_3	0.03	0.06	0.06	0.04	0.16	0.01	0.01	0.00	0.00	0.05	0.01	0.01
Fe_2O_3	7.23	3.38	3.83	4.10	3.29	6.19	4.88	5.68	4.42	6.44	5.73	7.34
FeO	3.77	1.41	2.78	1.83	1.40	1.86	2.70	2.14	2.87	2.23	2.61	1.86
MnO	0.19	0.14	0.11	0.12	0.11	0.17	0.15	0.24	0.16	0.19	0.16	0.19
MgO	10.24	15.52	13.47	14.58	15.64	13.11	13.50	12.83	13.22	12.44	12.00	11.43
CaO	23.54	23.61	23.26	23.39	23.75	22.11	22.39	22.16	22.89	22.13	22.48	22.62
Na_2O	0.32	0.33	0.42	0.37	0.32	0.80	0.57	0.79	0.59	0.77	0.70	0.62
K_2O	0.01	0.00	0.00	0.00	0.01	0.04	0.01	0.00	0.01	0.02	0.00	0.00
Sum	99.03	99.70	99.34	99.62	100.27	99.44	98.99	99.30	99.78	99.96	99.33	99.64
Site T												
Si	1.672	1.856	1.796	1.823	1.857	1.763	1.790	1.754	1.788	1.721	1.714	1.645
Al	0.328	0.144	0.204	0.177	0.143	0.237	0.210	0.246	0.212	0.279	0.286	0.355
Site M1												
Mg	0.589	0.800	0.739	0.785	0.826	0.721	0.739	0.698	0.724	0.671	0.663	0.627
Fe^{2+}	0.107	0.026	0.058	0.033	0.025	0.040	0.044	0.034	0.056	0.033	0.049	0.032
Mn	0.000	0.000	0.000	0.000	0.000	0.000	0.000	0.000	0.000	0.000	0.000	0.000
Fe^{3+}	0.208	0.094	0.107	0.114	0.090	0.164	0.138	0.160	0.124	0.180	0.162	0.208
Al	0.044	0.031	0.062	0.047	0.035	0.044	0.045	0.072	0.061	0.072	0.075	0.071
Cr	0.001	0.002	0.002	0.001	0.004	0.000	0.000	0.000	0.000	0.002	0.000	0.000
Ti	0.050	0.020	0.031	0.020	0.019	0.035	0.035	0.036	0.035	0.041	0.050	0.061
Site M2												
Ca	0.964	0.930	0.928	0.926	0.930	0.926	0.898	0.887	0.911	0.883	0.903	0.910
Na	0.023	0.024	0.031	0.027	0.023	0.042	0.041	0.057	0.043	0.056	0.051	0.045
Mn	0.006	0.004	0.003	0.004	0.003	0.006	0.005	0.007	0.005	0.006	0.005	0.006
Fe^{2+}	0.013	0.020	0.029	0.024	0.018	0.018	0.041	0.033	0.033	0.036	0.033	0.026
Mg	0.000	0.022	0.009	0.019	0.026	0.008	0.015	0.016	0.008	0.019	0.008	0.019
Wo	51.25	48.39	49.55	48.61	48.49	47.78	47.77	48.34	48.95	48.30	49.53	49.95
En	30.99	44.28	39.94	42.20	44.42	39.41	40.11	38.91	39.33	37.75	36.81	35.13
Fs	17.76	7.34	10.52	9.19	7.09	12.81	12.13	12.75	11.71	13.95	13.66	14.93
R^{3+}	0.303	0.147	0.202	0.182	0.148	0.243	0.218	0.268	0,220	0.295	0,287	0,340
Mg#	0.831	0.946	0.895	0.932	0.951	0.926	0.897	0.912	0.891	0.907	0.890	0.915

Trace Element Chemistry of Clinopyroxenes

Table 3 presents trace element and REE contents of four clinopyroxenes, selected from tephrite (Ktu1 and Yb11) in Group A, ol-tephrite (Yb6) in Group B and alkaline basalt (E6) in Group C of the NAVs. The chondrite-normalized (Boynton 1984) rare earth element patterns of the clinopyroxenes and their host rocks are similar to each other. They display strong enrichment in LREE relative to MREE and HREE, and compared to those of OIB-source (Figure 9a). The abundances of La and Ce were found to be ~200 times higher, and Yb and Lu ~10 times higher in the clinopyroxenes than those of the chondritic values. Moreover, compared to mantle clinopyroxenes with $(La/Lu)_N$ <1 (Cohen *et al.* 1984), the studied clinopyroxenes were found to have extremely fractionated REE patterns with $(La/Lu)_N$ ratios of 16–20.

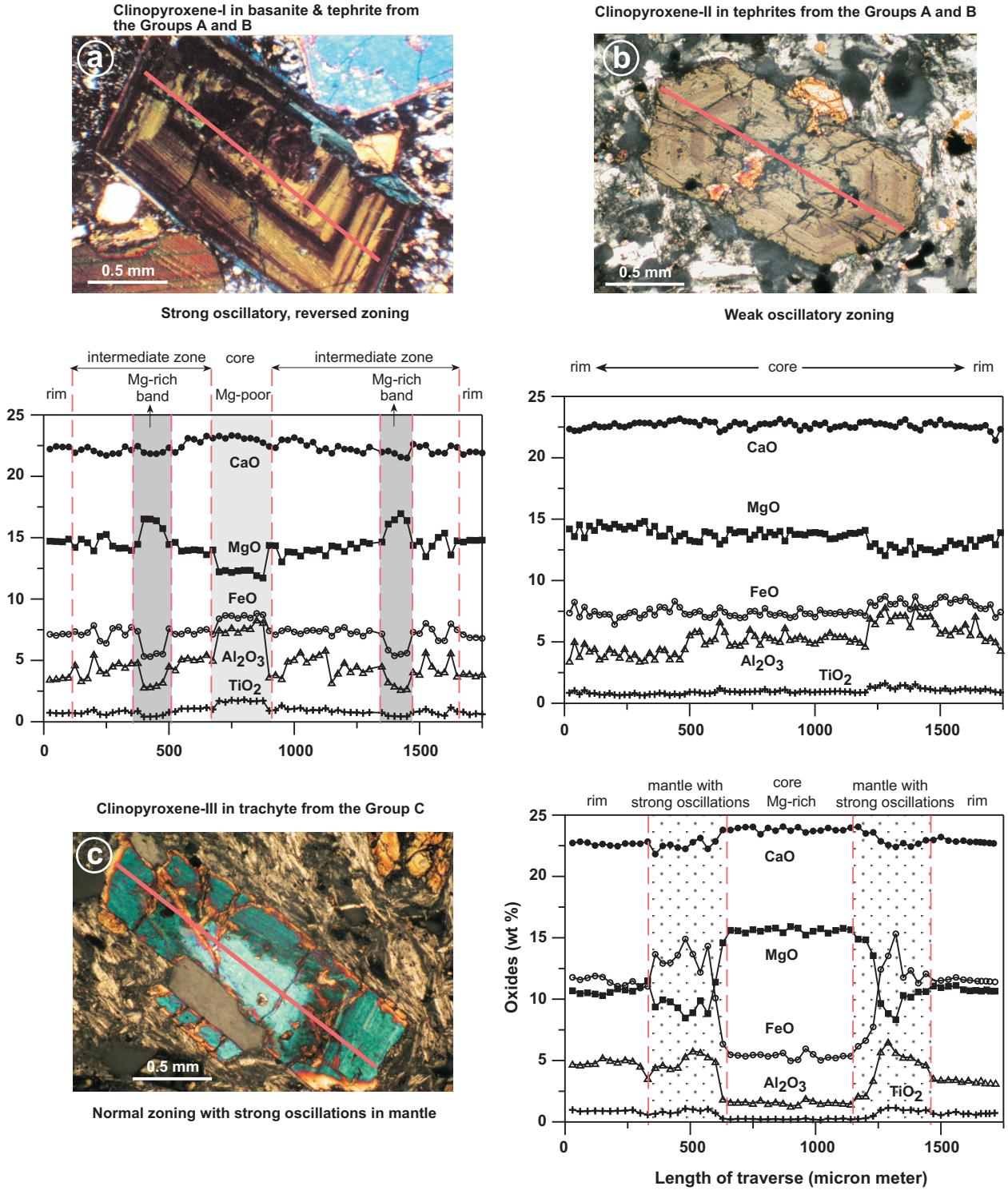

Figure 7. Compositional variations (MgO, CaO, FeO, Al_2O_3 and TiO_2) along a rim-to-rim traverse across for oscillatory zoned clinopyroxene phenocrysts (Cpx-I, Cpx-II and Cpx-III).

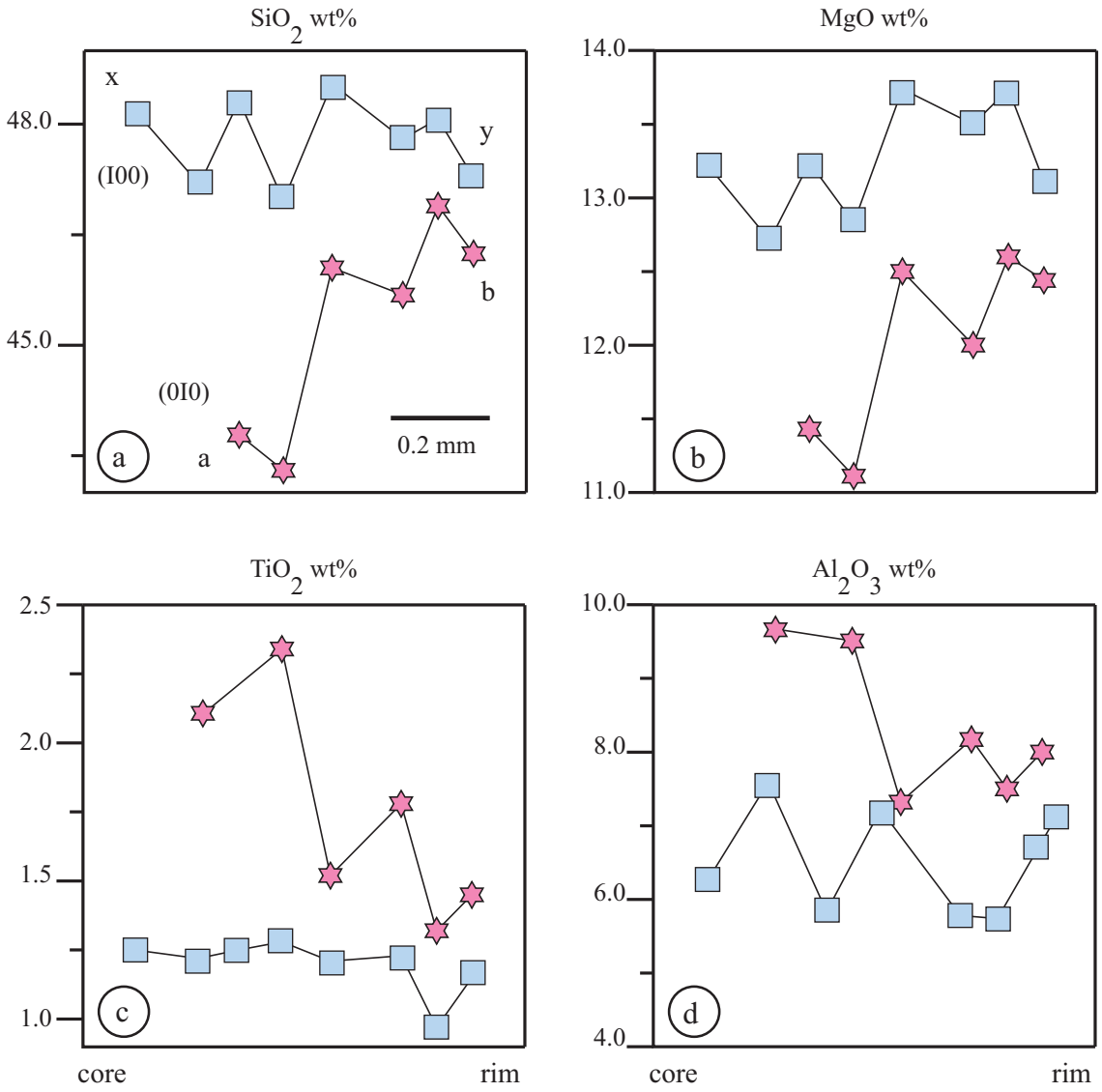

Figure 8. Compositional variations (SiO_2, MgO, TiO_2 and Al_2O_3) along a core-to-rim traverse across for a sector zoning clinopyroxene phenocryst.

The primitive mantle-normalized (Taylor & McLennan 1985) trace element patterns of the clinopyroxenes are also similar to each other with negative anomalies for Ti, Zr and Sr (Figure 9b), which were also observed in LREE-rich clinopyroxenes from Sicily, Italy (Nimis & Vannucci 1995) and clinopyroxenes from Warrumbungle Volcano, New South Wales, Australia (Ghorbani & Middlemost 2000). Another feature is the positive Sr anomaly in the host rocks, coupled with a negative Sr anomaly in the clinopyroxenes (Figure 9b).

Discussion

P-T Conditions of Clinopyroxenes

The investigated clinopyroxenes mostly fall in the 'igneous rocks' field of Aoki & Shiba (1973) on a $Al^{[6]}$ vs $Al^{[4]}$ diagram. Their $Al^{[6]}/Al^{[4]}$ ratios are generally lower than 0.25, which indicate relatively low-pressure crystallization (Figure 10a). They differ from those in xenoliths of mantle lherzolite (Dawson 1987) and high-pressure clinopyroxenes (Simonetti *et al.* 1996) in having lower Mg# (0.68–0.95, Figure 10b) and very low Cr_2O_3 (0.0–

Table 3. Trace element and REE contents of clinopyroxene phenocrysts from each series of the NAVs.

Lithology	Feldspar-free (A)	Feldspar- and Foid-bearing (B)		Feldspathoid-free (C)
	Tephrite	Tephrite		Alkaline basalt
Sample No	Ktu1	Yb11	Yb6	E6
Rb	0.76	< 0.3	0.95	0.35
Sr	885	982	1588	966
Y	28.7	32.0	32.4	30.8
Zr	305	330	258	319
Nb	4.83	4.91	4.14	4.81
Cs	<0.02	<0.02	<0.02	<0.02
Ba	24.0	10.6	172	12.7
Hf	8.47	8.51	6.83	8.47
Ta	0.64	0.67	0.52	0.64
Pb	1.64	0.90	2.13	1.64
Th	2.72	2.95	2.45	2.72
U	0.79	1.33	3.07	0.79
La	69.9	74.8	62.2	72.3
Ce	187	199	163	195
Pr	26.8	28.7	22.8	28.1
Nd	116	123	97.3	122
Sm	20.2	21.7	17.3	21.7
Eu	5.06	5.42	4.46	5.36
Gd	13.3	13.9	12.3	14.0
Tb	1.44	1.55	1.41	1.53
Dy	6.89	7.53	7.24	7.42
Ho	1.10	1.24	1.23	1.21
Er	2.80	3.10	3.20	3.02
Tm	0.35	0.38	0.40	0.36
Yb	2.12	2.41	2.47	2.28
Lu	0.32	0.35	0.35	0.34
Th/Y	0.09	0.09	0.08	0.09
Nb/Y	0.17	0.15	0.13	0.16
Rb/Y	0.03	< 0.01	0.03	0.01

Concentrations in ppm.

0.2 wt%, Figure 10b), Al_2O_3 (<9.6 wt%), and Na_2O (<0.9 wt%) contents.

A more quantitative estimate of pressure can be acquired with the equations proposed by Nimis (1995, 1999, 2000). In this study, we calculated the pressure by using the cpx-geobarometer proposed by Nimis (2000), which can be applied for basic tholeiitic to alkaline magmas with a standard error on pressure estimation within ±1.7 kbar. The equilibrium temperatures were estimated using the equation based on experimental work of McCallister *et al.* (1976) and on the method of Dal Negro *et al.* (1982). The chemical variations between the core and rim compositions of the clinopyroxenes in the each series do not affect significantly the estimated equilibrium pressures and intracrystalline closure temperatures, leading to a range of 2.9 – 4.6 ± 0.9 kbars and 946 – 949 ± 8 °C for the core compositions and of 2.4 – 4.1 ± 1.0 kbars and 941 – 962 ± 10 °C for the rim compositions (Table 4). However, the values of the core pressures in Group C clinopyroxenes are relatively lower (2.9±0.9 kbars) than those in Group A (4.0±0.7 kbars) and Group B (4.6±1.2 kbars). The estimated pressures approximately correspond to a crystallization depth of 11–14 ± 3 km for Groups A and B, and 7–9 ± 3 km for Group C, suggesting that these magma chambers in the Pontide crust were shallow.

There appear to be few differences between the estimated pressures derived from the Na-Mg# variation diagram (Figure 10c) and those from calculations (Table 4). In particular, while the Na content suggests that some

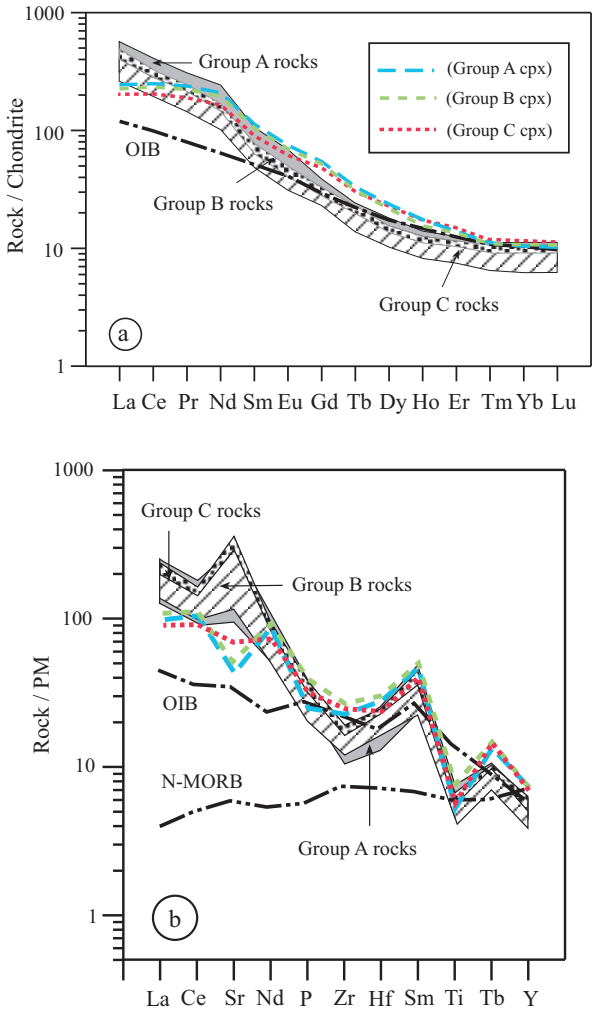

Figure 9. (a) Chondrite-normalized (Boynton 1984) REE patterns of the clinopyroxene phenocrysts in each series of the NAVs are compared with their host-rocks (shaded area). Data for host-rock compositions are from Aydin *et al.* (2008). (b) Primitive mantle-normalized (Taylor & McLennan 1985; Sr, Zr and Ti from Sun & McDonough 1989) multi element patterns of the clinopyroxene phenocrysts in each series. N-MORB from Saunders & Tarney (1984) and OIB from Sun (1980) and Sun & McDonough (1989).

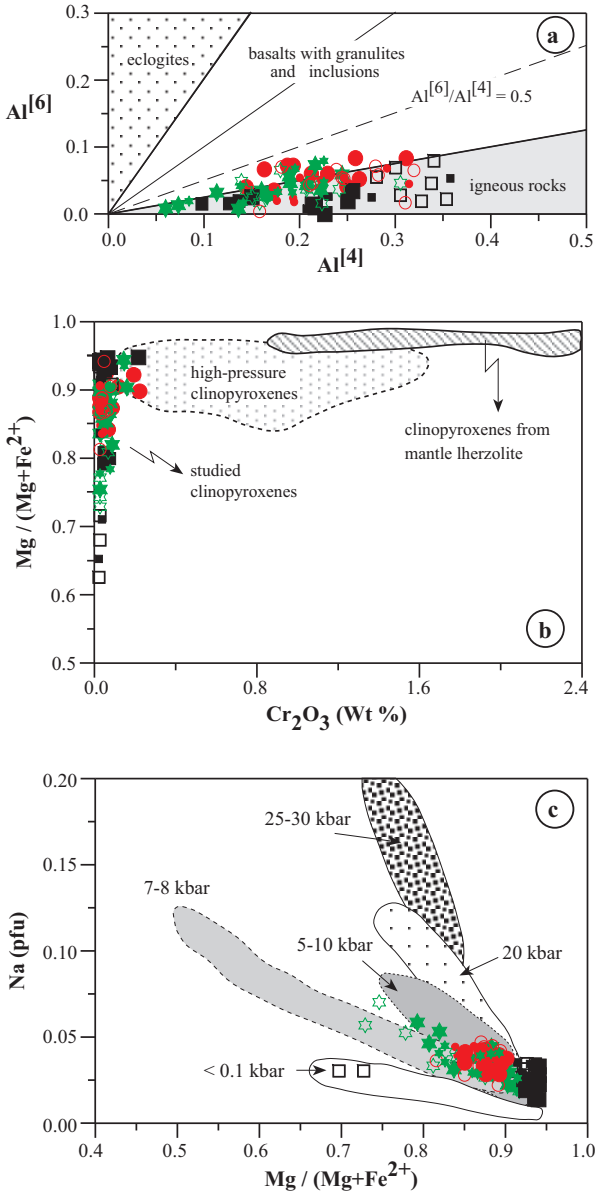

Figure 10. (a) $Al^{[6]}$ versus $Al^{[4]}$ plot of the studied clinopyroxenes. Boundary lines among the fields for clinopyroxenes in eclogites, granulites and inclusions in basalts and in igneous rocks are taken from Aoki & Shiba (1973). (b) Plot of Mg# = [Mg / ($Mg+Fe^{2+}$)] vs Cr_2O_3 (wt%) plots of the studied clinopyroxenes. Fields of clinopyroxenes from mantle lherzolite and high-pressure environment are taken from Dawson (1987) and Simonetti *et al.* (1996), respectively. (c) Mg# versus Na (a.f.u.) of the studied clinopyroxenes compared to clinopyroxenes with different pressures from various localities worldwide [high-pressure cpx data from Esin (1993) and Akinin *et al.* (2005); low-pressure clinopyroxenes data from Righter & Carmichael (1993); Dobosi & Jenner (1999)]. Symbols are as in Figure 3b.

pressure values range from 5 and 10 kbars, the quantitative results (Table 4), mostly based on Ti, Cr and $Al^{[6]}$ contents, are less than 5 kbars. Therefore, these studied clinopyroxenes have lower Na content than clinopyroxene phenocrysts from other locations, and thus do not resemble the high-pressure (>10 kbars) ones (Esin 1993; Akinin *et al.* 2005). In addition, relatively low Mg numbers (3.0–5.5) and Cr/(Cr+Al) ratios (1.9–2.8) of the spinels (Aydin *et al.* 2008) co-existing with the studied

Table 4. Estimated pressures (P), depths (D) and temperatures (T) of clinopyroxenes from each series of the NAVs.

	Feldspar-free Series (Group A)		Feldspar- and Foid-bearing Series (Group B)		Feldspathoid-free series (Group C)	
sample no rock types	P9a, Ktu1 basanite and tephrite		Yb6, Yb10, E10 tephrite and phonotephrite		E6, P9b alkaline basalt and trachybasalt	
	Cpx-core (n = 4)	Cpx-rim (n = 4)	Cpx-core (n = 6)	Cpx-rim (n = 5)	Cpx-core (n = 3)	Cpx-rim (n = 3)
P (kbar)[a]	4.0 ± 0.7	3.8 ± 0.7	4.6 ± 1.2	4.1 ± 1.7	2.9 ± 0.9	2.4 ± 0.9
D (km)	11.9 ± 2.0	11.3 ± 2.2	13.8 ± 3.5	12.3 ± 5.1	8.6 ± 2.9	7.2 ± 2.6
T (°C)[b]	946 ± 11	941 ± 10	947 ± 7	949 ± 9	949 ± 6	962 ± 12

[a] The pressures calculated using the cpx-geobarometer proposed by *Nimis* (2000). [b] For the intracrystalline equilibrium temperatures used the equation based on experimental work of *McCallister* et al. (1976) and the method of *Dal Negro* et al. (1982).

clinopyroxenes also support moderate- to low-pressure crystallization rather than a high-pressure origin.

Causes of Zoning Types in Clinopyroxenes

Various hypotheses can be considered to explain the occurrence of different zoning types in the studied clinopyroxenes.

A possible hypothesis is that the core and rim compositions of the clinopyroxenes crystallized at different pressures (Wass 1979; Dobosi & Horvath 1988). Figure 10a–c shows different diagrams for the cores and rims of the clinopyroxenes, and for groundmass crystals. These diagrams provide useful information about the crystallization pressure of clinopyroxenes, and show that there is little difference between the crystallization pressures of the cores and rims of the studied clinopyroxenes. Based on the cpx-barometer of Nimis (2000), pressure values (2.4–4.6 ± 0.9 kbars) of the clinopyroxenes (rims and cores) calculated here are consistent with the pressure data (estimated from core-compositions of the cpx-crystals) from Aydin *et al.* (2008). Obtained results indicate that (i) there is no considerable variation in crystallization pressure between the cores and rims of the clinopyroxenes (Table 4), (Figure 10a–c), and (ii) the cores and rims of the clinopyroxenes are likely to have crystallized in a moderate- to low-pressure environment (~5–2 kbars).

The other alternative hypotheses are that the studied clinopyroxenes are of xenocrystic (mantle or magmatic xenocrysts; Shaw & Eyzaguirre 2000) or co-magmatic (Vollmer *et al.* 1981; Barton *et al.* 1982) origin (i.e. a magma mixing/mingling process). As xenocrysts are not in chemical and/or textural equilibrium with the melt, they react or are resorbed within the melt. In addition, no xenocrysts of other mineral phases or remnants of xenoliths are present in the alkaline volcanics. However, magma mixing has been recognized as one of the main processes that can induce disequilibrium phenomena such as complex or reverse zoning and resorption/reaction textures. Indeed, most disequilibrium textures are ascribed to magma mixing by many researchers (Wass 1979; Duda & Shimincke 1985; Dobosi & Fodor 1992; Simonetti *et al.* 1996). Such a process is known to be able to generate strong heterogeneities within magma bodies on very short scales (e.g., Perugini *et al.* 2002, 2003). However, textural and crystal chemical studies reveal that most clinopyroxenes (all samples in Group A and some of the samples in Groups B and C) in each series of the NAVs are in equilibrium with the melt (Figure 6) and show strong compositional similarities (Figures 4, 5, 9 & 10), which all reflect a common petrogenetic affinity. On the other hand, the Mg-rich clinopyroxenes in Groups B and C probably represent earlier-crystallized phenocrysts from deeper and higher-MgO magmas predating the equilibrium phenocrysts that occur in the same samples.

A further hypothesis is that the studied clinopyroxene phenocrysts are cognate-type xenoliths as suggested by Şen (2000). He also stated that these clinopyroxenes were not mantle xenoliths and they formed during the halts of magma ascent, based on mineralogical and mineral chemical data. Consequently, these clinopyroxenes represent early crystals precipitated from a parental magma (probably alkaline basaltic magma),

produced by low degree of partial melting of an enriched and young lithospheric mantle (0.51–0.59 Ga) (Aydin *et al.* 2008). The heat source of melting was related to asthenospheric upwelling induced by lithospheric delamination, resulting from the extensional tectonic regime in the eastern Pontides during Middle Miocene–Pliocene time (Aydin *et al.* 2008). Such a process, occurring with decompression crystallization, is likely to lead to compositional variations in the studied clinopyroxenes with oscillatory (normal and reverse), sectorial and normal zoning at moderate- to low-pressure (~5–2 kbars). In addition, the resorption texture of core parts of some clinopyroxene phenocrysts and skeletal olivines from the Groups A and B rock series (Figure 2e, f) can also be attributed to the abrupt changes of crystallization pressure (i.e. decompression) due to the similar core and rim compositions rather than magma mixing. Consequently, the alkaline basaltic magma started to crystallize with the precipitation of clinopyroxene ± olivine at mid-crustal depths, followed by moderate to low-pressure fractionation during magma ascent into a shallow magma chamber in the upper crust. Subsequently, in the evolved part of the alkaline magma clinopyroxene phenocrysts were produced with oscillatory (normal and reverse), sectorial and normal zoning by a relatively low-pressure fractionation process following the different crystallization paths (Hoskin *et al.* 1998a, b) and the variations in fluid regime of the melt (Aydin *et al.* 2000, 2001).

Petrogenetic Implication and Modelling

Both trace and rare earth element contents of the clinopyroxenes and their host whole-rock compositions provide important information on initial melt compositions and magma evolution (Dobosi & Jenner 1999; Bizimis *et al.* 2000). As clinopyroxene is one of the earliest crystallization products, its composition reflects the original (less fractionated and contaminated) magma composition, and provides some information about the possible directions of melt evolution. Closed or open-system effects on magma evolution can be recorded by trace element compositions in clinopyroxene and its host-melt (Wood & Blundy 1997; Vanucci *et al.* 1998). For example, constant compositions or similar LILE- and LREE enrichments in the clinopyroxenes and their host-rocks will reflect closed-system behaviour. By contrast, considerable differences between trace element contents of the clinopyroxenes and their host-rocks will chemically reveal an open system.

Based on the primitive mantle and chondrite-normalized trace and rare earth element patterns (Figure 9a, b), the studied clinopyroxenes and their host rocks show rather similar element abundance patterns, with enrichment in LREE (e.g., La, Ce) and negative Ti and Zr anomalies, except for Sr which was enriched in the host-rocks by the presence of Sr-rich feldspars (Aydin *et al.* 2003b). The similar clinopyroxene patterns imply that parental magmas of the clinopyroxenes may be derived from a similar source, and may have experienced the low-pressure crystallization processes in closed magma chambers. The relatively flat HREE distribution patterns in chondrite-normalized diagrams (Figure 9), show that HREE fractionations, are weak and do not support the presence of garnet in the mantle source region. Hence, according to REE partial melting models (Şen *et al.* 1998), the alkaline rocks could also have been produced by 5–10% partial melting of a highly metasomatised spinel mantle source. The clinopyroxenes also have relatively low ratios of Nb/Y (≈ 0.1–0.2) and Th/Y (< 0.1) (Table 3) compared to the host-rocks (Nb/Y ≈ 1.0–2.0; Th/Y ≈ 0.4–1.0), and to OIB (Nb/Y ≈ 5.0; Th/Y ≈ 0.5) (Aydin *et al.* 2008). In these subduction-related magmas, these data and the host-rock geochemical fingerprints such as high LILE/HFSE ratios and the negative Nb, Ta and Ti anomalies indicate the presence of metasomatic components in the source potassic alkaline magmas, which originated from lithospheric mantle enriched by earlier subduction. Host-rock compositions and isotope ratios are, moreover, inconsistent with assimilation crystallization (AFC) or magma mixing processes (Aydin *et al.* 2008). Instead, all data obtained from this study are more consistent with the presence of relatively low-pressure fractional crystallization in closed-magma chambers during the evolution of the alkaline magma.

Based on the textural features and compositions of the clinopyroxenes, a schematic section of the magmatic system is depicted in Figure 11, and its petrogenetic model can be introduced as follows. Initially, alkaline basaltic magma was derived from a lithospheric mantle, already enriched by previous subduction processes. This magma rapidly rose towards the surface, resulting from an extensional tectonic regime, and reached the mid-crustal level (Figure 11). Then, the basic magma started

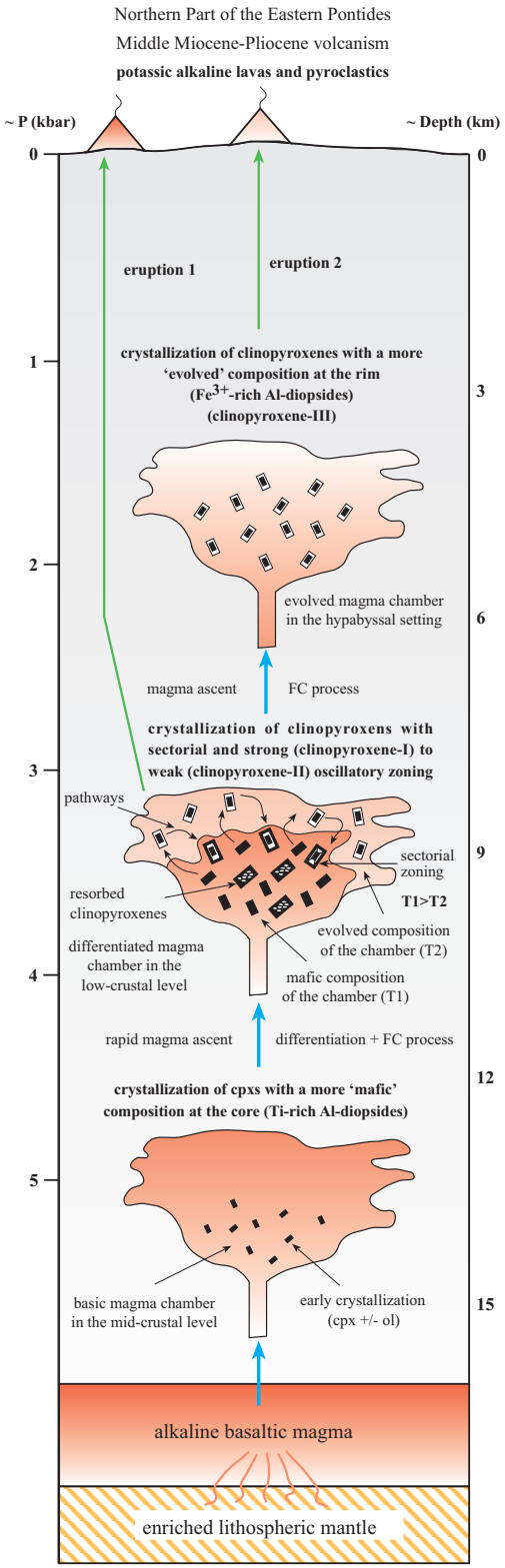

Figure 11. Schematic illustration for the evolution and crystallization processes of alkaline magma within the eastern Pontide crust.

to crystallize at depth ~15 km and ~5–6 kbars (quantitatively estimated from the cpx-barometer). During this stage, clinopyroxenes with more 'mafic' cores (Ti-rich Al-diopside) and Mg-rich olivines ± Fe-Ti oxides crystallized in the magma chamber. Rapid ascent of the magma then continued, reaching a shallower depth in the crust (~9–10 km). At this stage, the rising magma stagnated and started to differentiate in a closed-system (mafic and evolved composition in Figure 11). During this stage, sectorial and oscillatory zoned clinopyroxenes (Clinopyroxenes-I and Clinopyroxenes-II; Figure 7a, b) and resorbed clinopyroxenes with skeletal olivines started to crystallize due to undercooling or decompression crystallization (Nelson & Montana 1992; Hammer & Rutherford 2002). Decompression crystallization can cause heating of the magma due to release of latent heat (Blundy *et al.* 2006), and thus, lead to increasing Mg contents during clinopyroxene crystallization. Stagnation, subsequent cooling and degassing at the water-saturation point may lead to lower Mg content as observed in the Clinopyroxenes-I (Figure 7a). Subsequently, the evolved part of the magma (probably trachytic in composition) separated and rose to form a shallower magma reservoir (i.e. shallower or hypabyssal setting). During this stage, clinopyroxenes (Clinopyroxenes-III; Figure 7c) with a more 'evolved' composition at the rim (Fe-rich Al-diopside) crystallized in the chamber. Finally, the system began to stabilize with the formation of rim compositions of the clinopyroxenes. Based on the composition of clinopyroxenes, it is estimated that the pre-eruptive temperatures (i.e. intracrystalline equilibrium temperatures) were in the range of ~940–960 °C (Table 4).

Conclusions

Based on the compositions (major and trace elements) and zoning types of the clinopyroxenes from the different series of the NAVs from the eastern Pontides, NE-Turkey, the following concluding remarks can be made.

1. Clinopyroxene phenocrysts (Ti-rich Al-diopside to Fe^{3+}-rich Al-diopside) are cognate-type xenoliths, (i.e. they crystallized as early crystals during a pause in the ascent of magma into the upper crust), and show mostly strong compositional and textural similarities, suggesting a common crystallization and petrogenetic history.

2. Pre-eruptive temperature and pressure values, estimated from the clinopyroxene geothermo-barometer for the NAVs, are in the range of 940–960 °C and ~2–5 kbars, respectively, supporting moderate to low-pressure crystallization in shallow magma chambers in the Pontide crust at a nearly constant temperature.
3. The compositional trends of the clinopyroxenes indicate three types of zoning: (i) oscillatory and sectorial zoning related to melt crystallization, (ii) oscillatory and reverse zoning related to the different crystallization paths under a variable fluid regime, (iii) normal zoning related to the fractional crystallization during ascent of the magma.
4. The zoning types and compositional variations show evidence of different crystallization stages observed in the cores, mantles and rims of the clinopyroxenes, and probably reflect the variations in fluid regime of the melt during fractionation and ascent of the alkaline magma within the Pontide crust.
5. Due to the similar core and rim compositions, the resorption texture of core parts of some clinopyroxenes and skeletal olivine phenocrysts are attributed to the changes of crystallization pressure (i.e. decompression) though such textures have been ascribed to magma mixing.
6. Based on chondrite-normalized trace and REE patterns, all the clinopyroxenes have high abundances of LREE with negative HFSE anomalies, suggesting a common source (probably alkaline basaltic magma) derived from a young and homogeneous lithospheric mantle enriched by an earlier subduction event. The alkaline magma produced then underwent a relatively low-pressure fractionation in closed magma chambers at different levels accounting for the variations in the crystallization conditions during rapid magma ascent, in the post-collision extensional tectonic regime which affected the eastern Pontides during Middle Miocene-Pliocene time.

Acknowledgments

This work, produced partially from the corresponding author's PhD Thesis, was fully supported by the Scientific Research Projects Funding Center of Karadeniz Technical University, and by a grant from Deutscher Akademischer Austauschdienst (DAAD). The authors would like to give special thanks to Rainer Altherr (Mineralogisches Institut, Universität Heidelberg, Germany) for his permission to use the electron microprobe. Hans-Peter Meyer (Mineralogisches Institut, Universität Heidelberg, Germany) and Gültekin Topuz (Eurasia Institute of Earth Sciences, İstanbul Technical University, Turkey) are thanked for their assistance with electron microprobe analyses. Many thanks are given to Peter Möller and Peter Dulski (GeoForschungsZentrum, German Research Centre for Geosciences, Potsdam, Germany) for the trace element and REE analyses. The authors also thank the referees who are Fatma Toksoy Köksal and two anonymous scientists for their precious and kind contributions to improve the quality of the paper. The English of the final text is edited by John A. Winchester.

References

Akin, H. 1979. Geologie, magmatismus und Lagerstattenbildung im ostpontischen Gebirge/Türkei aus der Sicht der Plattentektonik. *Geolgische Rundschau* **68**, 253–283.

Akinin, V.V., Sobolev, A.V., Ntaflos, T. & Richter, W. 2005. Clinopyroxene megacrysts from Enmelen melanophelinitic volcanoes (Chukchi Peninsula, Russia): application to composition and evolution of mantle melts. *Contributions to Mineralogy and Petrology* **150**, 85–101.

Aldanmaz, E. 2006. Mineral-chemical constraints on the Miocene calc-alkaline and shoshonitic volcanic rocks of Western Turkey: disequilibrium phenocryst assemblages as indicators of magma storage and mixing conditions. *Turkish Journal of Earth Sciences* **15**, 47–73.

Aoki, K. & Shiba, I. 1973. Pyroxenes from lherzolite inclusions of Itinomegata, Japan. *Lithos* **6**, 41–51.

Aurisicchio, C., Federico, M. & Gianfagna, A. 1988. Clinopyroxene chemistry of the high-potassium suite from the Alban Hills, Italy. *Mineralogy and Petrology* **39**, 1–19.

Avanzinelli, R., Bindi, L., Menchetti, S. & Conticelli, S. 2004. Crystallisation and genesis of peralkaline magmas from Pantelleria Volcano, Italy: an integrated petrological and crystal-chemical study. *Lithos* **73**, 41–69.

Aydin, F. 2003. *Değirmendere Vadisi (Trabzon-Esiroğlu, KD-Türkiye) Volkanitlerinin Mineral Kimyası, Petrolojisi and Petrojenezi [Mineral Chemistry, Petrology and Petrogenesis of the Değirmendere Valley Volcanics (Trabzon-Esiroğlu, NE-Turkey)].* PhD Thesis, Karadeniz Technical University, Trabzon, Turkey [in Turkish with English abstract, unpublished].

AYDİN, F. 2008. Contrasting complexities in the evolution of calc-alkaline and alkaline melts of the Niğde volcanic rocks, Turkey: textural, mineral chemical and geochemical evidence. *European Journal of Mineralogy* **20**, 101–118.

AYDİN, F., KARSLI, O. & CHEN, B. 2008. Petrogenesis of the Neogene alkaline volcanics with implications for post-collisional lithospheric thinning of the Eastern Pontides, NE Turkey. *Lithos* **104**, 249-266.

AYDİN, F., KARSLI, O. & SADIKLAR, M.B. 2000. Petrologic significance of the complexly zoned clinopyroxenes in the volcanic rocks from Eastern Pontides (NE-Turkey). *Beihefte zum European Journal of Mineralogy* **12**, p. 5.

AYDİN, F., KARSLI, O., SADIKLAR, M.B. & ALTHERR, R. 2001. Mineralogy and chemical characteristics of the sector and oscillatory zoned diopsides from Pliocene alkaline volcanic suites, South of Trabzon/NE-Turkey. *Beihefte zum European Journal of Mineralogy* **13**, p. 17.

AYDİN, F., KARSLI, O. & SADIKLAR, M.B. 2003a. Mineralogy and chemistry of biotites from Eastern Pontide granitoid rocks, NE Turkey: Some petrological implications for granitoid magmas. *Chemie der Erde- Geochemistry* **63**, 163–182.

AYDİN, F., KARSLI, O., SADIKLAR, M.B. & ALTHERR, R. 2003b. Chemical characteristics and crystallization temperature of Ba- and Sr-rich feldspar minerals from undersaturated alkaline volcanics, Trabzon, NE-Turkey. *Beihefte zum European Journal of Mineralogy* **15**, p. 10.

BARBIERI, M., CONFORTO, L., GARBARINO, C., MASI, U., NICOLETTI, M. & AKINCI, Ö. 2000. Geo-chemistry of hydrothermally-altered volcanic rocks of the upper volcanic cycle from the Eastern Pontides (Northeastern Turkey). *Chemie der Erde- Geochemistry* **60**, 81–95.

BARTON, M. & VAREKAMP, J.C. & VAN BERGEN, M.J. 1982. Complex zoning of clinopyroxenes in the lavas of Vulsini, Latium, Italy: evidence for magma mixing. *Journal of Volcanology and Geothermal Research* **14**, 361–388.

BINDI, L., CELLAI, D., MELLUSO, L., CONTICELLI, S., MORRA, V. & MENCHETTI, S. 1999. Crystal chemistry of clinopyroxene from alkaline undersaturated rocks of the Monte Vulture Volcano, Italy. *Lithos* **46**, 259–274.

BIZIMIS, M., VINCENT, J.M.S. & ENRICO, B. 2000. Trace and REE content of clinopyroxenes from supra-subduction zone peridotites: implications for melting and enrichment processes in island arcs. *Chemical Geology* **165**, 67–85.

BOYNTON, W.V. 1984. Geochemistry of the rare earth elements: meteorite studies. *In:* HENDERSON, P. (ed), *Rare Earth Element Geochemistry*, Elsevier, 63–114.

BOZKURT, E. 2001. Neotectonics of Turkey – a synthesis. *Geodinamica Acta* **14**, 3–30.

BOZTUĞ, D., JONCKHEERE, R., WAGNER, G.A. & YEĞENGİL, Z. 2004. Slow Senonian and fast Palaeocene–Early Eocene uplift of the granitoids in the Central Eastern Pontides, Turkey: apatite fission-track results. *Tectonophysics* **382**, 213–228.

BOZTUĞ, D., ERÇİN, A.İ., KURUÇELİK, M.K., GÖÇ, D., KÖMÜR, İ. & İSKENDEROĞLU, A. 2006. Main geochemical characteristics of the composite Kaçkar batholith derived from the subduction through collision to extensional stages of Neo-Tethyan convergence system in the Eastern Pontides, Turkey. *Journal of Asian Earth Sciences* **27**, 286–302.

BOZTUĞ, D., JONCKHEERE, R., WAGNER, G.A., ERÇİN, A.İ. & YEĞİNGİL, Z. 2007. Titanite and zircon fission-track dating resolves successive igneous episodes in the formation of the composite Kaçkar batholith in the Turkish eastern Pontides. *International Journal of Earth Sciences* **96**, 875–886.

BLUNDY, J., CASHMAN, K. & HUMPHYRES, M. 2006. Magma heating by decompression-driven crystallization beneath andesite volcanoes. *Nature* **443**, 76–80.

CANIL, D. & FEDORTCHOUCK, Y. 2000. Clinopyroxene-liquid partitioning for vanadium and the oxygen fugacity during formation of cratonic and oceanic mantle lithosphere. *Journal of Geophysical Research* **105**, 26003–26016.

COHEN, R.S., O'NIONS, R.K. & DAWSON, J.B. 1984. Isotope geochemistry of xenoliths from East Africa: implications for development of mantle reservoirs and their interaction. *Earth and Planetary Science Letters* **68**, 209–220.

ÇAMUR, Z., GÜVEN, İ.H. & ER, M. 1996. Geochemical characteristics of the Eastern Pontide volcanics, Turkey: an example of multiple volcanic cycles in the arc evolution. *Turkish Journal of Earth Sciences* **5**, 123–144.

DAL NEGRO, A., CARBONIN, S., MOLIN, G.M., CUNDARI, A. & PICCIRILLO, E.M. 1982. Intracrystalline cation distribution in natural clinopyroxenes of tholeiitic, transitional, alkaline basaltic rocks. *In:* SAXENA, S.K. (ed), *Advances in Physical Geochemistry*. Springer, New York, 117–150.

DAL NEGRO, A., CUNDARI, A., PICCIRILLO, E.M., MOLIN, G.M. & ULIANA, D. 1986. Distintive crystal chemistry and site configuration of the clinopyroxene from alkaline basaltic rocks: the Nyambeni clinopyroxene suite Kenya. *Contributions to Mineralogy and Petrology* **92**, 35–43.

DAL NEGRO, A., MANOLI, S., SECCO, L. & PICCIRILLO, E.M. 1989. Megacrystic clinopyroxenes from Victoria (Australia): crystal chemical comparisons of pyroxenes from high and low pressure regimes. *European Journal of Mineralogy* **1**, 105–121.

DAWSON, J.B. 1987. Metasomatized harzburgites in kimberlite and alkaline magmas: enriched restites and 'flushed' lherzolites. *In:* MENZIES, M.A. & HAWKESWORTH, C.J. (eds), *Mantle Metasomatism*. Academic Press, London, 125–144.

DEER, W.A., HOWIE, R.A. & ZUSSMAN, J. 1978. *Rock-forming Minerals. 2nd Edition, Single-Chain Silicates, 2A*. Longman, London.

DOBOSI, G. & FODOR, F.V. 1992. Magma fractionation, replenishment, and mixing as inferred from green-core clinopyroxenes in Pliocene basanite, Southern Slovakia. *Lithos* **28**, 133–150.

DOBOSI, G. & HORVÁRTH, I. 1988. High- and low-pressure cognate clinopyroxenes from alkali lamprophyres of the Velence and Buda mountains, Hungary. *Neues Jahrbuch Fur Mineralogie-Abhandlungen* **158**, 241–256.

DOBOSI, G. & JENNER, G.A. 1999. Petrologic implications of trace element variation in clinopyroxene megacrysts from yhe Nógrád volcanic province, North Hungary: a study by laser ablation microprobe-inductively coupled plasma-mass spectrometry. *Lithos* **46**, 731–749.

DOWNES, M.J. 1974. Sector and oscillatory zoning in calcic augites from Mt. Etna, Sicily. *Contributions to Mineralogy and Petrology* **47**, 187–196.

DOWTY, E. 1976. Crystal structure and crystal growth: II. sector zoning in minerals. *American Mineralogist* **61**, 460–469.

DROOP, G.T.R. 1987. A general equation for estimating Fe^{3+} concentrations in ferromagnesian silicates and oxides from microprobe analyses, using stoichiometric criteria. *Mineralogical Magazine* **51**, 431–435.

DUDA, A. & SCHMINCKE, H.U. 1985. Polybaric differentiation of alkali basaltic magmas: evidence from green-core clinopyroxenes (Eifel, FRG). *Contributions to Mineralogy and Petrology* **91**, 340–353.

DULSKI, P. 2001. Reference materials for geochemical studies: new analytical data by ICP-MS and critical discussion of reference values. *Geostandards Newsletter-The Journal for Geostandards and Geoanalysis* **25**, 87–125.

EĞİN, D., HIRST, D.M. & PHILLIPS, R. 1979. The petrology and geochemistry of volcanic rocks from the northern Harşit river area, Pontide volcanic province, northeast Turkey. *Journal of Volcanological and Geothermal Research* **6**, 105–123.

ELBURG, M.A., BERGEN, M.V., HOOGEWERFF, J., FODEN, J., VROON, P., ZULKARNAIN, I. & NASUTION, A. 2002. Geochemical trends across an arc-continent collision zone: magma sources and slab-wedge transfer processes below the Pantar Strait volcanoes, Indonesia. *Geochimica et Cosmoschimica Acta* **66**, 2771–2789.

ESİN, S.V. 1993. *Injection Magmatism in Upper Mantle: Test of Empirical Clinopyroxene Geothermobarometer*. Siberian Branch of RAS, United Institute of Geology, Geophysics and Mineralogy, Novosibirsk.

FREY, F.A., GREEN, D.H. & ROY, S.D. 1978. Intergrated models of basalt petrogenesis: a study of quartz tholeiites to olivine melilites from southeastern Australia utilizing geochemical and experimental data. *Journal of Petrology* **19**, 463–513.

GHORBANI, M.R. & MIDDLEMOST, E.A.K. 2000. Geochemistry of pyroxene inclusions from the Warrumbungle Volcano, New South Wales, Australia. *American Mineralogist* **85**, 1349–1367.

GROVE, T.L., GERLACH, D.C. & SANDO, T.C. 1982. Origin of calc-alkaline series lavas at Medicine Lake volcano by fractionation, assimilation and mixing. *Contributions to Mineralogy and Petrology* **80**, 160–182.

HAMMER, J. & RUTHERFORD, M. 2002. An experimental study of the kinetics of decompression-induced crystallization in silicic melt. *Journal of Geophysical Research* **107**, 2021.

HAWKESWORTH, C.J., TURNER, S.P., MCDERMOTT, F., PEATE, D.W. & VAN CALSTEREN, P. 1997. U-Th isotopes in arc magmas: implications for element transfer from the subducted crust. *Science* **276**, 551–555.

HOSKIN, P.W.O. & WYSOCZANSKI, R.J. 1998. In situ accurate and precise lead isotopic analysis of ultra-small analytevolumes (10^{-16} m^3) of solid inorganic samples by high mass resolution secondary ion mass spectrometry. *Journal of Analytical Atomic Spectrometry* **13**, 597–601.

HOSKIN, P.W.O., ARSLAN, M. & ASLAN, Z. 1998a. Clinopyroxene phenocryst formation in an alkaline magma: interpretations from oscillatory zoning. *Goldschmidt Conference, Mineralogical Magazine Abstracts* **62**, 653–654.

HOSKIN, P.W.O., YAXLEY, G.M., ARSLAN, M. & ASLAN, Z. 1998b. Clinopyroxene phenocrysts in basaltic alkaline magmas: chemical and optical zoning. *Geological Society of New Zealand, Joint Annual Conference Abstracts*, p. 124.

KARSLI, O., AYDİN, F. & SADIKLAR, M.B. 2002. Geothermobarometric investigation of the Zigana Granitoid, eastern Pontides, Turkey. *International Geology Review* **44**, 277–286.

KARSLI, O., AYDİN, F. & SADIKLAR, M.B. 2004a. Magma interaction recorded in plagioclase zoning in granitoid systems, Zigana Granitoid, Eastern Pontides, Turkey. *Turkish Journal of Earth Sciences* **13**, 287–305.

KARSLI, O., AYDİN, F. & SADIKLAR, M.B. 2004b. The morphology and chemistry of K-feldspar megacrysts from İkizdere Pluton: evidence for acid and basic magma interactions in granitoid rocks, NE Turkey. *Chemie der Erde-Geochemistry* **64**, 155–170.

KARSLI, O., CHEN, B., AYDIN, F. & ŞEN, C. 2007. Geochemical and Sr-Nd-Pb isotopic compositions of the Eocene Dölek and Sariçiçek plutons, Eastern Turkey: Implications for magma interaction in the genesis of high-K calc-alkaline granitoids in a post-collision extensional setting. *Lithos* **98**, 67–96.

KESKİN, M. 2003. Magma generation by slab steepening and breakoff beneath a subduction-accretion complex: An alternative model for collision-related volcanism in Eastern Anatolia, Turkey. *Geophysical Research Letters* **30** (24), 8046. doi:10.1029/2003GL018019.

KORKMAZ, S. 1993. Tonya-Düzköy (GB Trabzon) yöresinin stratigrafisi [Stratigraphy of the Tonya-Düzköy (SW Trabzon) area, NE Turkey]. *Geological Bulletin of Turkey* **36**, 151–158 [in Turkish with English abstract].

LETERRIER, J., MAURY, R.C., THONON, P., GIRARD, D. & MARCHAL, M. 1982. Clinopyroxene composition as a method of identification of the magmatic affinities of paleo-volcanic series. *Earth and Planetary Science Letters* **59**, 139–154.

LIOTARD, J.M., BRIOT, D. & BOIVIN, P. 1988. Petrological and geochemical relationships between pyroxene megacrysts and associated alkali-basalts from Massif Central xenolith suite (France). *Contributions to Mineralogy and Petrology* **98**, 81–90.

MALGAROTTO, C., MOLIN, G. & ZANAZZI, F. 1993. Crystal chemistry of clinopyroxenes from Filicudi and Salina (Aeolian Islands, Italy): geothermometry and barometry. *European Journal of Mineralogy* **5**, 915–923.

MANOLI, S. & MOLIN, G.M. 1988. Crystallographic procedures in the study of experimental rocks: X-ray single-crystal structure refinement of C2/c clinopyroxene from Lunar 74275 high-pressure experimental basalt. *Mineralogy and Petrology* **39**, 187–200.

McCallister, R.H., Finger, L.W. & Ohashi, Y. 1976. Intracrystalline Fe^{2+}-Mg equilibria in three natural Ca-rich clinopyroxenes. *American Mineralogist* **61**, 671–676.

Morimoto, N., Fabries, J., Ferguson, A.K., Ginzburg, I.V., Ross, M., Seifert, F.A., Zussman, J., Aoki, K. & Gottardi, G. 1988. Nomenculature of pyroxenes. *American Mineralogist* **73**, 1123–1133.

Nakamura, Y. 1973. Origin of sector-zoning of igneous clinopyroxenes. *American Mineralogist* **58**, 986–990.

Nazzareni, S., Molin, G., Peccerillo, A. & Zanazzi, P.F. 2001. Volcanological implications of crystal-chemical variations in clinopyroxenes from the Aeolian Arc, Southern Tyrrhenian Sea (Italy). *Bulletin of Volcanology* **63**, 73–82.

Nelson, S.T. & Montana, A. 1992. Sieve-textured plagioclase in volcanic rocks produced by rapid decompression. *American Mineralogist* **77**, 1242–1249.

Nimis, P. 1995. A clinopyroxene geobarometer for basaltic systems based on crystal structure modelling. *Contributions to Mineralogy and Petrology* **121**, 115–125.

Nimis, P. 1999. Clinopyroxene geobarometry of magmatic rocks: Part 2 – structural geobarometers for basic to acid, tholeiitic and mildly alkaline magmatic systems. *Contributions to Mineralogy and Petrology* **135**, 62–74.

Nimis, P. 2000. CpxBar-Excel version program. Available from <http://dmp.unipd.it/Nimis/ researche.html>.

Nimis, P. & Vanucci, R. 1995. An ion microprobe study of clinopyroxenes in websteritic and megacrystic xenoliths from Hyblean Plateau (SE Sicily, Italy): constraints on HFSE/REE/Sr fractionation at mantle depth. *Chemical Geology* **124**, 185–197.

Nimis, P. & Ulmer, P. 1998. Clinopyroxene geobarometer of magmatic rocks. Part 1: An expanded structural geobarometer for anhydrous and hydrous, basic and ultrabasic systems. *Contributions to Mineralogy and Petrology* **133**, 122–135.

Okay, A.İ. 1989. Tectonic units and sutures in the Pontides, Northern Turkey. *In:* Şengör, A.M.C. (ed), *Tectonic Evolution of the Tethyan Region*. NATO ASI Series C **259**, 109–116.

Okay, A.İ. & Şahintürk, Ö. 1997. Geology of the Eastern Pontides. *In:* Robinson, A.G. (ed), *Regional and Petroleum Geology of the Black Sea and Surrounding Region*. AAPG Memoir **68**, 291–311.

Okay, A.İ., Şahintürk, Ö. & Yakar, H. 1997. Stratigraphy and tectonics of the Pulur (Bayburt) region in the eastern Pontides. *Bulletin of the Mineral Research and Exploration* **119**, 1–24.

Okay, A.İ., Bozkurt, E., Satır, M., Yiğitbaş, E., Crowley, Q.G. & Shang, C.K. 2008. Defining the southern margin of Avalonia in the Pontides: Geochronological data from the Late Proterozoic and Ordovician granitoids from NW Turkey. *Tectonophysics* **461**, 252–264.

Özsayar, T. 1987. Trabzon kıyı bölgesinde volkanitlerin yaşına ilişkin veriler [The evidence for the age of the volcanic rocks exposing along the coastal range, Trabzon]. *Geological Congress of Turkey, Ankara, Abstracts*, p. 37.

Papike, J.J., Cameron, K.L. & Baldwin, K. 1974. Amphiboles and pyroxenes: characterization of other than quadrilateral components and estimates of ferric iron from microprobe data. *Geology Society of America* **6**, 1053–1054.

Pearce, J.A. 1983. Role of the sub-continental lithosphere in magma genesis at active continental margins. *In:* Hawkesworth, C.J. & Norry, N.J. (eds), *Continental Basalts and Mantle Xenoliths*. Shiva, Cheshire, UK, 230–249.

Perini, G., Francalanci, L., Davidson, J.P. & Conticelli, S. 2004. Evolution and genesis of magmas from Vico volcano, central Italy: multiple differentiation pathways and variable parental magmas. *Journal of Petrology* **45**, 139–182.

Perugini, D., Poli, G. & Gatta, G.D. 2002. Analysis and simulation of magma mixing processes in 3D. *Lithos* **65**, 313–330.

Perugini, D., Busa, T., Poli, G. & Nazzareni, S. 2003. The role of chaotic dynamics and flow fields in the development of disequilibrium textures in volcanic rocks. *Journal of Petrology* **44**, 733–756.

Princivalle, F., Tirone, M. & Comin-Chiaramonti, P. 2000. Clinopyroxenes from spinel-peridotite mantle xenoliths from Nemby (Paraguay): crystal chemistry and petrological implications. *Mineralogy and Petrology* **70**, 25–35.

Righter, K. & Carmichael, I.S.E. 1993. Maga-xenocrysts in alkali olivine basalts: fragments of disrupted mantle assemblage. *American Mineralogist* **78**, 1230–1245.

Robinson, A.G., Banks, C.J., Rutherford, M.M. & Hirst, J.P.P. 1995. Stratigraphic and structural development of the Eastern Pontides, Turkey. *Journal of the Geological Society, London* **152**, 861–872.

Rolland, Y., Billo, S., Corsini, M., Sosson, M. & Galoyan, G. 2008. Blueschists of the Amassia-Stepanavan suture zone (Armenia): linking Tethys subduction history from E Turkey to W Iran. *International Journal of Earth Sciences*, doi: 10.1007/s00531-007-0286-8.

Saunders, A.D. & Tarney, J. 1984. Geochemical characteristics of basaltic volcanism within back-arc basins. *In:* Kokelaar, B.P. & Howells, M.F. (eds), *Marginal Basin Geology*. Geological Society, London, Special Publications **16**, 59–76.

Sazonova, L.V. & Nosova, A.A. 1999. Clinopyroxene zoning as an Indicator of the magmatic melt cooling conditions: an example of odinites from the Urals. *Geochemical International* **37**, 1141–1157.

Şen, C. 1994. *Subduction Related Petrologic Processes: 1- Dehydration Melting of a Basaltic Composition Amphibolite 2- Mantle Metasomatism*. PhD Thesis, University of New Brunswick, New Brunswick-Canada.

Şen, C. 2000. Petrography, mineralogy and chemistry of ultramafic nodules from volcanic rocks of post Eocene age, Eastern Pontide Alkaline Province (NE, Turkey). *Cumhuriyetin 75. Yıldönümü Yerbilimleri ve Madencilik Konferansı, MTA-Ankara, Proceedings*, 55–66 [in Turkish with English abstract].

Şen, C., Arslan, M. & Van, A. 1998. Geochemical and petrological characteristics of the Eastern Pontide Eocene (?) alkaline volcanic province, NE Turkey. *Turkish Journal of Earth Sciences* **7**, 231–239.

ŞENGÖR, A.M.C. & KIDD, W.S.F. 1979. Post-collisional tectonics of the Turkish-Iranian plateau and a comparison with Tibet. *Tectonophysics* **55**, 361–376.

ŞENGÖR, A.M.C. & YILMAZ, Y. 1981. Tethyan evolution of Turkey: A plate tectonic approach. *Tectonophysics* **75**, 181–241.

ŞENGÖR, A.M.C., GÖRÜR, N. & ŞAROGLU, F. 1985. Strike slip faulting and related basin formation in zones of tectonic escape: Turkey as a case study. *In:* BIDDLE, T.R. & CHRISTIE-BLICK, N. (eds), *Strike-slip Deformation, Basin Formation and Sedimentation*. International Journal of Society of Economic Paleontologists and Mineralogists, Special Publiciation **37**, 227–264.

ŞENGÖR, A.M.C., ÖZEREN, S., GENÇ, T. & ZOR, E. 2003. East Anatolian high plateau as a mantle-supported, North-south shortened domal structure. *Geophysical Research Letters* **30** (24), 8045, doi:10.1029/2003GL017858.

SHAW, C.S.J. & EYZAGUIRRE, J. 2000. Origin of megacrysts in the mafic alkaline lavas of the West Eifel volcanic field, Germany. *Lithos* **50**, 75–95.

SHEARER, C.K. & LARSEN, L.M. 1994. Sector-zoned aegirine from the Ilimaussaq alkaline intrusion. South Greenland: implications for trace element behaviour in pyroxene. *American Mineralogist* **79**, 340–352.

SHIMIZU, N. 1981. Trace element incorporation into growing augite phenocrysts. *Nature* **289**, 575–577.

SHIMIZU, N. 1990. The oscillatory trace element zoning of augite phenocrysts. *Earth Science Review* **29**, 27–37.

SIMONETTI, A., SHORE, M. & BELL, K. 1996. Diopside phenocrysts from nephelinite lavas, Napak Volcano, Eastern Uganda: Evidence for magma mixing. *Canadian Mineralogist* **34**, 411–421.

SISSON, T.W. & GROVE, T.L. 1993. Experimental investigations of the role of H_2O in calc-alkaline differentiation and subduction zone magmatism. *Contributions to Mineralogy and Petrology* **113**, 143–166.

SUN, S.S. 1980. Lead isotopic study of young volcanic rocks from mid-ocean ridges, ocean islands and island arcs. *Philosophical Transactions of the Royal Society A* **297**, 409–445.

SUN, S.S. & MCDONOUGH, W.F. 1989. Chemical and isotopic systematics of oceanic basalts: implications for mantle composition and processes. *In:* SAUNDERS, A.D. & NORRY, M.J. (eds), *Magmatism in the Ocean Basins.* Geological Society, London, Special Publications **42**, 313–345.

TAYLOR, S.R. & MCLENNAN, S.M. 1985. *The Continental Crust: Its Composition and Evolution*. Blackwell, Oxford, London.

TOKEL, S. 1977. Eocene calc-alkaline andesites and geotectonism in the eastern Black Sea Region. *Geological Bulletin of Turkey* **20**, 49–54 [in Turkish with English Abstract].

TOPLIS, M.J. & CARROL, M.R. 1995. An experimental study of the influence of oxygen fugacity on Fe-Ti oxide stability, phase relations, and mineral-melt equilibria in ferro-basaltic systems. *Journal of Petrology* **36**, 1137–1170.

TOPUZ, G. & ALTHERR, R. 2004. Pervasive rehydration of granulites during exhumation – an example from the Pulur complex, Eastern Pontides, Turkey. *Mineralogy and Petrology* **81**, 165–185.

TOPUZ, G., ALTHERR, R., KALT, A., SATIR, M., WERNER, O. & SCHWARZ, W.H. 2004a. Aluminous granulites from the Pulur complex, NE Turkey: a case of partial melting, efficient melt extraction and crystallision. *Lithos* **72**, 183–207.

TOPUZ, G., ALTHERR, R., SATIR, M. & SCHWARZ, W.H. 2004b. Low-grade metamorphic rocks from the Pulur complex, NE-Turkey: implications for the pre-Liassic evolution of the Eastern Pontides. *International Journal of Earth Sciences* **93**, 72–91.

TOPUZ, G., ALTHERR, R., SCHWARZ, W.H., SIEBEL, W., SATIR, M. & DOKUZ, A. 2005. Post-collisional plutonism with adakite-like signatures: the Eocene Saraycık granodiorite (Eastern Pontides, Turkey). *Contributions to Mineralogy and Petrology* **150**, 441–455.

VANUCCI, R., BOTTAZZI, P., WULFF-PEDERSEN, E. & NEUMANN, E.-R. 1998. Partitioning of REE, Y, Sr, Zr and Ti between clinopyroxene and silicate melts in the mantle under La Palma (Canary Islands): implications for the nature of the metasomatic agents. *Earth and Planetary Science Letters* **158**, 39–51.

VOLLMER, R., JOHNSTON, K., GHIARA, M.R., LIRER, L. & MUNNO, R. 1981. Sr isotope geochemistry of megacrysts from continental rift and converging plate margin alkaline volcanism in South Italy. *Journal of Volcanology and Geothermal Research* **11**, 317–327.

WASS, S.Y. 1979. Multiple origins of clinopyroxene in alkalic basaltic rocks. *Lithos* **12**, 115–132.

WATSON, E.B. & LIANG, Y. 1995. A simple model for sector zoning in slowly grown crystals: implications for growth rate and lattice diffusion, with emphasis on accessory minerals in crustal rocks. *American Mineralogist* **80**, 1179–1187.

WESTAWAY, R. 1994. Present-day kinematics of the Middle East and Eastern Mediterranean. *Journal of Geophysical Research* **99**, 12071–12090.

WOOD, B.J. & BLUNDY, J.D. 1997. A predictive model for rare earth element partitioning between clinopyroxene and anhydrous silicate melt. *Contributions to Mineralogy and Petrology* **129**, 166–181.

YILMAZ, C., ŞEN, C. & ÖZGÜR, S. 2001. Timing of the earliest andesitic volcanic activity in the eastern Pontide volcanic arc. *International Earth Science Colloquium on the Aegean Region, İzmir-Turkey, Proceedings*, 47–55.

YILMAZ, S. & BOZTUĞ, D. 1996. Space and time relations of three plutonic phases in the Eastern Pontides, Turkey. *International Geological Review* **38**, 935–956.

YILMAZ, Y. 1993. New evidence and model on the evolution of the Southeast Anatolian orogen. *Geology Society of American Bulletin* **105**, 251–271.

YILMAZ, Y., TÜYSÜZ, O., YİĞİTBAŞ, E., GENÇ, S.C. & ŞENGÖR, A.M.C. 1997. Geology and tectonic evolution of the Pontides. *In:* ROBINSON, A.G. (ed), *Regional and Petroleum Geology of the Black Sea and Surrounding Region*. AAPG Memoir **68**, 183–226.

ZHU, Y.-F. & OGASAWARA, Y. 2004. Clinopyroxene phenocrysts (with green salite cores) in trachybasalts: implications for two magma chambers under the KokcheNAPV UHP massif, North Kazakhstan. *Journal of Asian Earth Sciences* **22**, 517–527.